ANNUAL PROGRESS REPORT

TO

THE UNITED STATES ATOMIC ENERGY COMMISSION

CONTRACT AT(30-1) 3510

BIOLOGICAL AND CLINICAL DOSIMETRY

Contract Period: November 1, 1967 - October 31, 1968

Report Period: July 1, 1967 - June 30, 1968

Senior Investigator: John S. Laughlin, Ph.D., Member

Sloan-Kettering Institute for Cancer Research
410 East 68th Street, New York 21, New York

DISCLAIMER

4. Evaluation of matrix response to low energy gamma rays using detector cooling

5. Evaluation of commercially produced instrumentation for use with matrix arrays

6. Effect of restorative surface treatments on matrix properties

B. Experimental Tests of Ultrasonic Bonding of Electrical Lead Wires to Diode Electrodes

1. Applications planned
2. Results

C. Construction of Miniature pn Junction Silicon Diodes with Ultrasonically Bonded Leads.

I. SUMMARY

A highly accurate output monitor system utilizing a current transformer was developed for the 30 nanosecond pulse field emission electron source. Charge and energy fluence were determined as a function of distance from the source. Dose rate dependence was studied for rates up to 3 x 10^{12} Rads/sec for LiF and CaF_2:Mn thermoluminescent dosimeters. Depth dose measurements were made in polystyrene using microtomed teflon CaF_2:Mn dosimeters.

Preliminary experiments were performed with the dual channel 2 nanosecond pulse field emission electron source.

The results of our participation in the National Bureau of Standards (NBS) electron beam dosimetry uniformity study are discussed.

An ionization chamber has been fabricated from Shonka tissue equivalent plastic for measurement of total tissue dose and depth dose distributions produced by fast neutrons.

A matrix of lithium drifted diodes consisting of a single square diode 1.6 cm on a side and 3 mm depletion depth was made to yield incident beta particle position within 3 mm^2. The matrix configuration results from the formation of effectively isolated detection regions on the single compensated region. The partitioning geometry admits the practicality of assembling such devices into larger arrays for mapping the distribution of extended radioactive sources. Measurements of matrix electrical characteristics are presented.

Miniature pn junction silicon diodes were produced for eventual in vivo applications. The use of ultrasonic bonding techniques facilitated the attachment of .005" aluminum electrical lead wires which are expected to minimize the effects of scattering from lead wires on diode response in irradiated media.

II. DOSIMETRY OF ULTRAHIGH INTENSITY ELECTRON SOURCES

A. Introduction

Electron generators operating on the field emission principle are capable of producing very high doses and dose rates (1,2). The nature of these sources, however, is such that pulse to pulse as well as long-term variations in output can occur. Consequently, the development of a suitable monitoring system is necessary for satisfactory application of these generators to problems of radiation biology and radiation effects.

In this report, the development of a non-intercepting monitoring system for a 600 KeV field emission electron source producing 30 nanosecond pulses will be described together with thermoluminescent dosimetry studies utilizing this system. Initial experience with a generator producing 3 nanosecond pulses will also be discussed. Some of the material in this report has been presented at meetings of the American Association of Physicists in Medicine and the Radiation Research Society (3,4).

B. Experimental Arrangement for Development of Monitoring System for the 30 Nanosecond Pulsed Source

The Field Emission Corporation Model 701 600 KeV electron generator produces single pulses of 1000 amperes and 30 nanosecond duration. Correspondingly, doses greater than 10^5 rads and dose rates in excess of 10^{12} rad/sec are obtained. Output variations of as much as ± 15% can occur in a given series of pulses, and long-term drift of the average output is also observed.

Because of the extremely high intensity and short duration, conventional ionization chambers cannot be used. The relatively low energy of the electron beam indicates the desirability of a non-intercepting type of monitor. A current monitoring transformer was chosen, since it has been shown (5,6,7) that such a monitor could be used with high precision. The use of a current monitoring transformer for such short non-repetitive current pulses is unique, since previous work dealt with pulses which were either both long (∿1μsec) and/or repetitive. Two commercially manufactured transformers (Model No. 110A and 2100, Pearson Electronics Inc.) were evaluated.

A block diagram of the experimental apparatus is shown in Figure 1. The electron beam passes coaxially through the aperture of the current transformer. The output of the current transformer is then integrated and the peak height of the integrated pulse measured with a peak reading memory voltmeter. The monitor output is compared with the energy deposition measured by an intensity calorimeter, or with the charge collected on the calorimeter wafer. The charge is integrated on a capacitor and the voltage developed read with an electrometer.

Due to the large amount of RF noise present when the machine is fired, it was found necessary to delay the current transformer pulse with a coaxial delay line about 1.5 μsec long. The monitor readout and integrator are housed in an RF shielded enclosure. The AC power for the monitor system is derived from a battery pack and inverter to isolate the monitor system from power line noise. Aluminum shields prevent stray electrons from striking the current transformer. Electrons hitting the inner shield are returned to ground in the opposite direction to cancel the voltage they induced originally. A beam stop was incorporated to reduce the RF noise generated when the beam is stopped in air.

C. Intensity Calorimeter

Because of the relatively low kinetic energy of the electrons and the high flux produced by the field emission generator, the design of the calorimeter to measure pulse intensity is not elaborate. The calorimeter consists of a 3 mm thick by 35 mm diameter aluminum wafer suspended on nylon monofilaments inside an aluminum vacuum jacket. The calorimeter with vacuum jacket removed is shown in Figure II. The electrons enter the calorimeter through a .05 mm mylar vacuum window and, with the exception of those backscattered, are totally absorbed. The aluminum wafer contains a single thermistor to monitor temperature changes and four small precision resistors to permit calibration by depositing a known amount of energy in the calorimeter electrically. A lead is also provided to return the stopped electrons to ground, or to the integrating capacitor.

Figure I

BLOCK DIAGRAM OF MONITOR SYSTEM

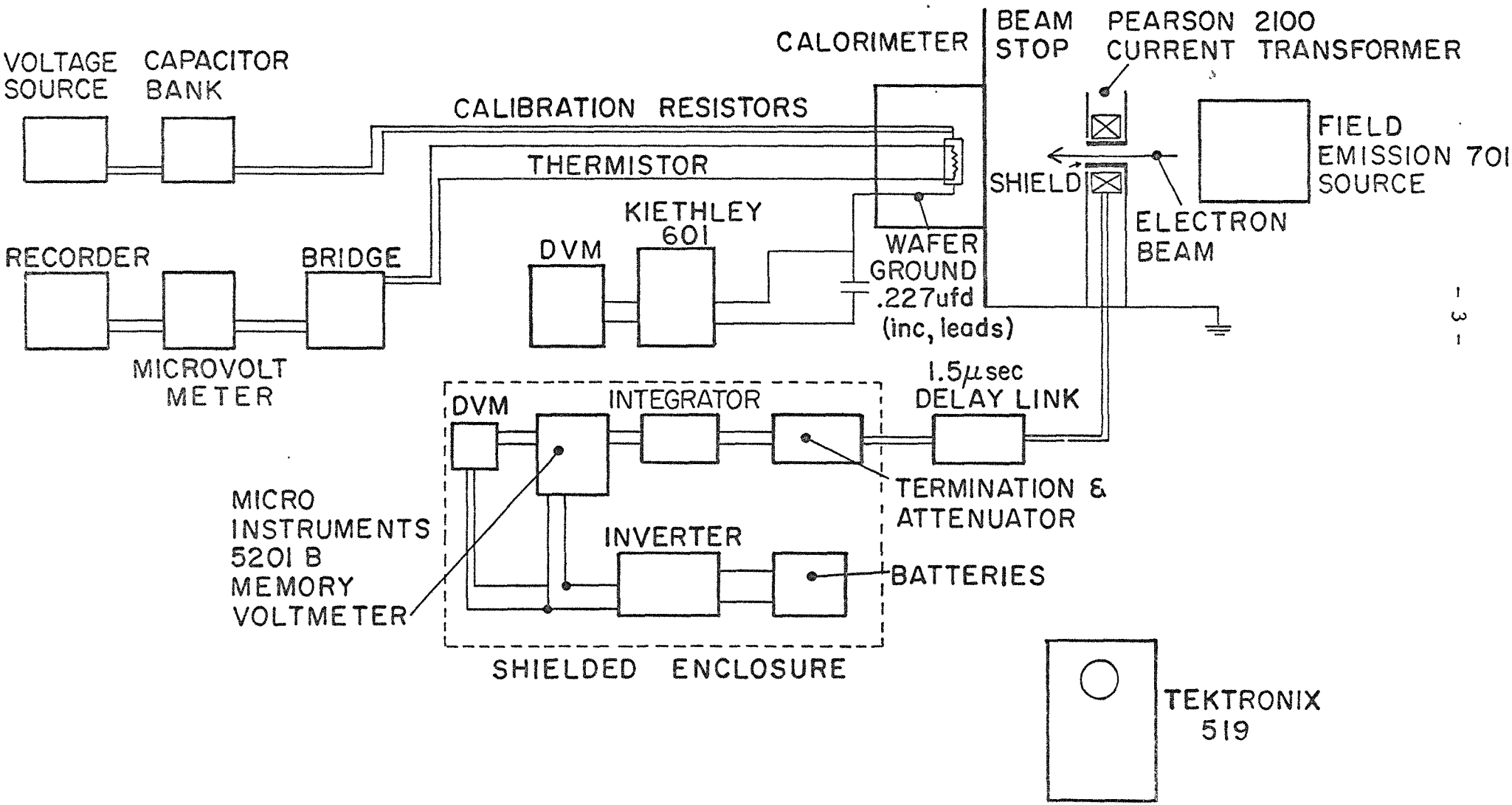

FIGURE II

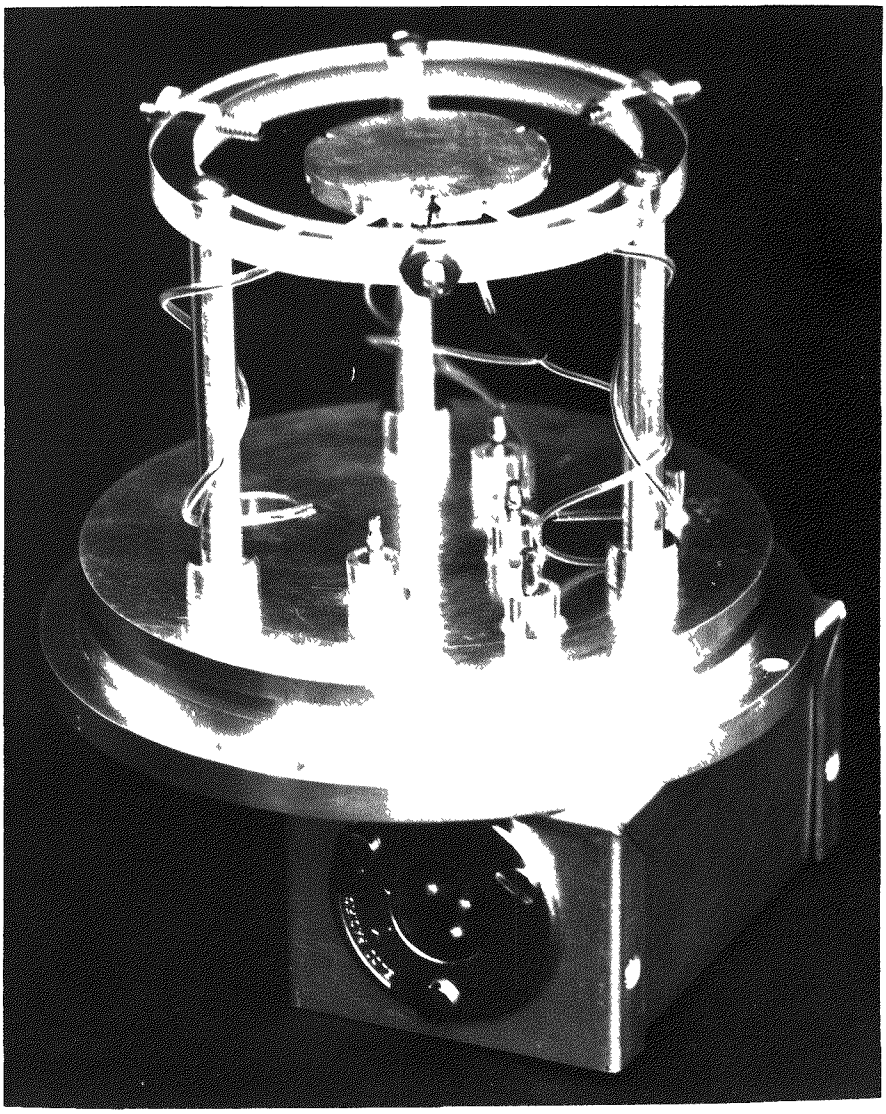

INTENSITY CALORIMETER
(VACUUM JACKET REMOVED)

Since the temperature changes in the calorimeter produced by the electron beam are of the pulse type, this is simulated in the calibration by the discharge of a capacitor bank charged to a known voltage. In this way, the energy input necessary to produce a given fractional change in thermistor resistance can be determined. Figure III shows typical calibration data, giving the variation in calibration factor with energy input. Allowing for a reproducibility of about ± 1.0% these data indicate that over a range from 16 millijoules to 1.6 joules, the calibration factor is constant, and consequently the calorimeter response is linear with energy.

D. Current Transformer Monitor Operation

An oscillo gram of the output of the current transformer at 20 nanosec/cm sweep rate is shown in Figure IV. The current pulse width appears to be approximately 50 nanoseconds at half-width, which is wider than the manufacturer's quoted pulse width. The dispersion of the delay line, however, broadens the pulse. Because of the short pulse duration, operational amplifier integrators are not applicable and attempts at using charge storage integrators were unsatisfactory due to difficulty in locating a suitable low forward resistance fast diode. The fact that the pulse is singly occurring prevents the use of sampling techniques.

These problems were circumvented by the use of a matched filter to integrate the current pulse. It can be shown that the peak output of a matched filter is proportional to the area under the input pulse. Unfortunately, an exactly matched filter cannot be made for our pulse shape. One must therefore approximate the current pulse by another for which a matched filter can be made. A decaying exponential (τ = 44 nsec) was chosen. Figure V compares the decaying exponential with the current pulse. A matched filter for the decaying $A = e^{-t/\tau}$ is an RC integrator with time constant τ. The integrator output is shown in Figure VI (100 nsec/cm). The pulse width is approximately 100 nsec at 50% points.

Since it is possible to measure simultaneously intercepted energy, collected charge and monitor output for each pulse, one can calibrate the monitor in terms of either energy or charge. One also has the information to determine how charge collected by the calorimeter is related to the energy deposited.

E. Calibration Results

The integrated current transformer output was compared with both the average beam intensity and charge collected on the calorimeter at various distances from the tube window. The reproducibility of the system was evaluated by taking identical sets of data on different days. In Figures VII and VIII, typical sets of measurements have been fitted by least squares straight lines. The data points are seen to lie within ± 1.5% error bands.

The choice of a linear representation was one of convenience since analysis of the data taken indicates the existence of non-zero intercepts of considerable magnitude which are constant regardless of distance. Since both the response of the calorimeter and the integrator voltmeter combination can be demonstrated to be linear through the origin within experimental limits, a

Figure III

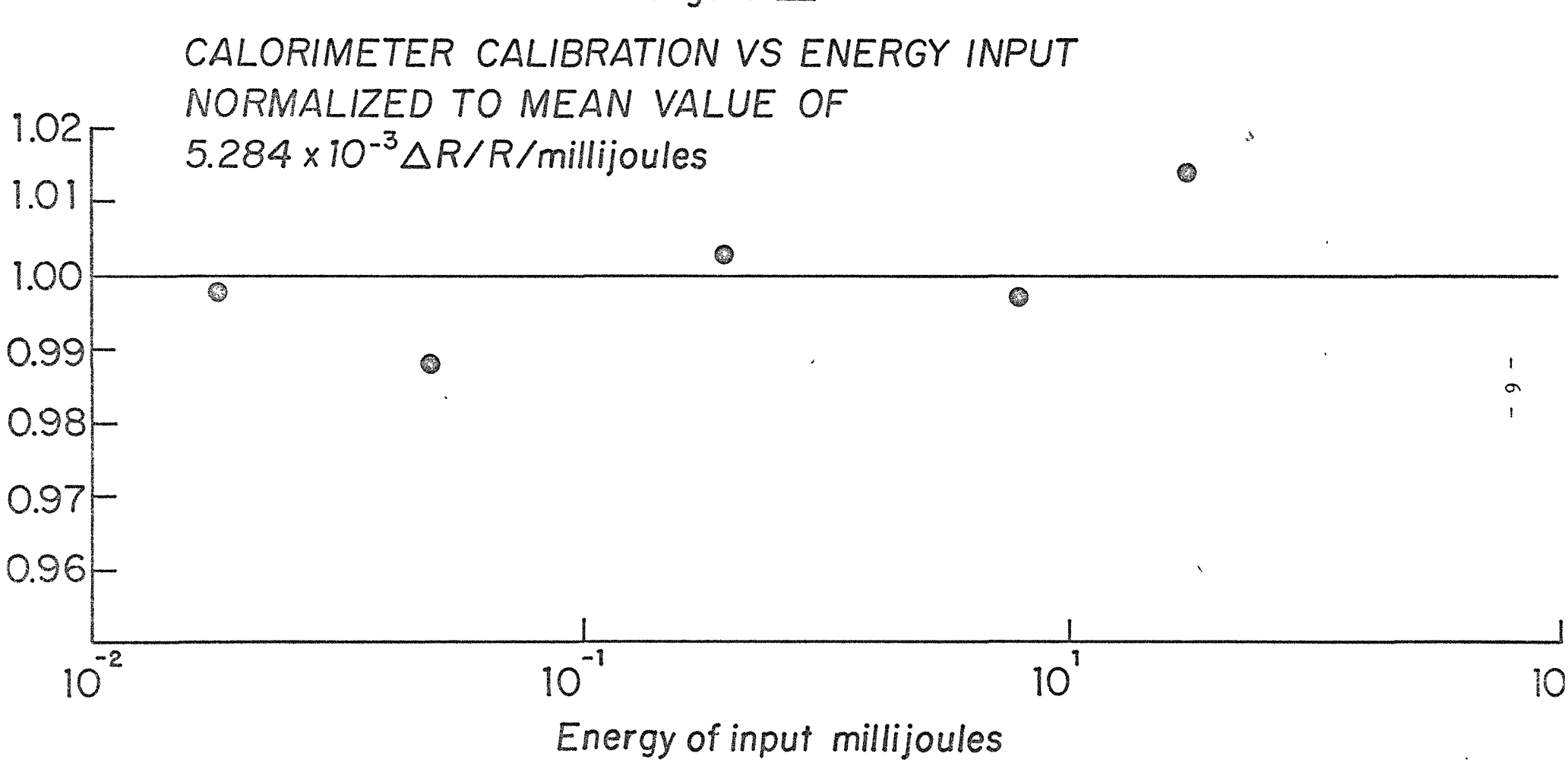
CALORIMETER CALIBRATION VS ENERGY INPUT
NORMALIZED TO MEAN VALUE OF
5.284 x 10^-3 ΔR/R/millijoules
1.02
1.01
1.00
0.99
0.98
0.97
0.96
10^-2
10^-1
10^1
10
Energy of input millijoules

FIGURE IV

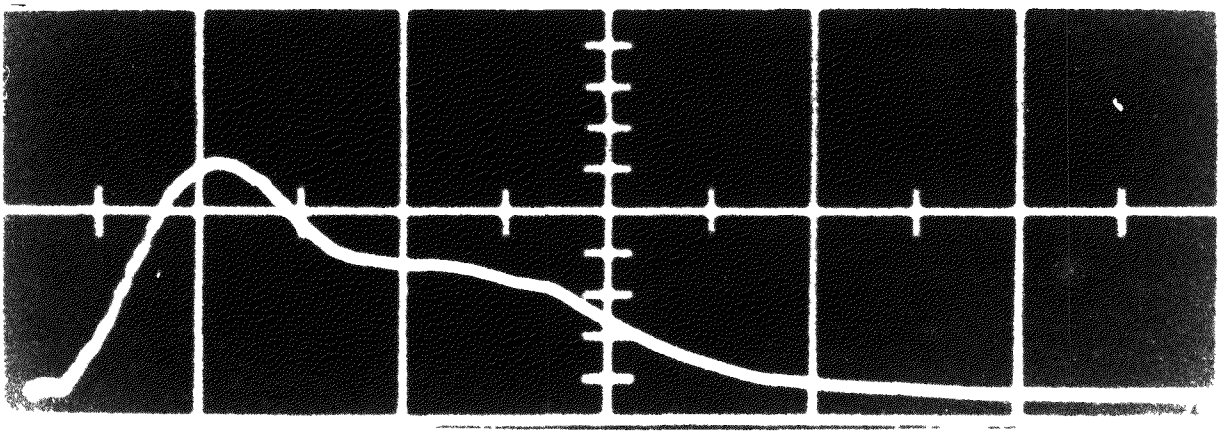

CURRENT TRANSFORMER OUTPUT
20 NSEC/CM

Figure V

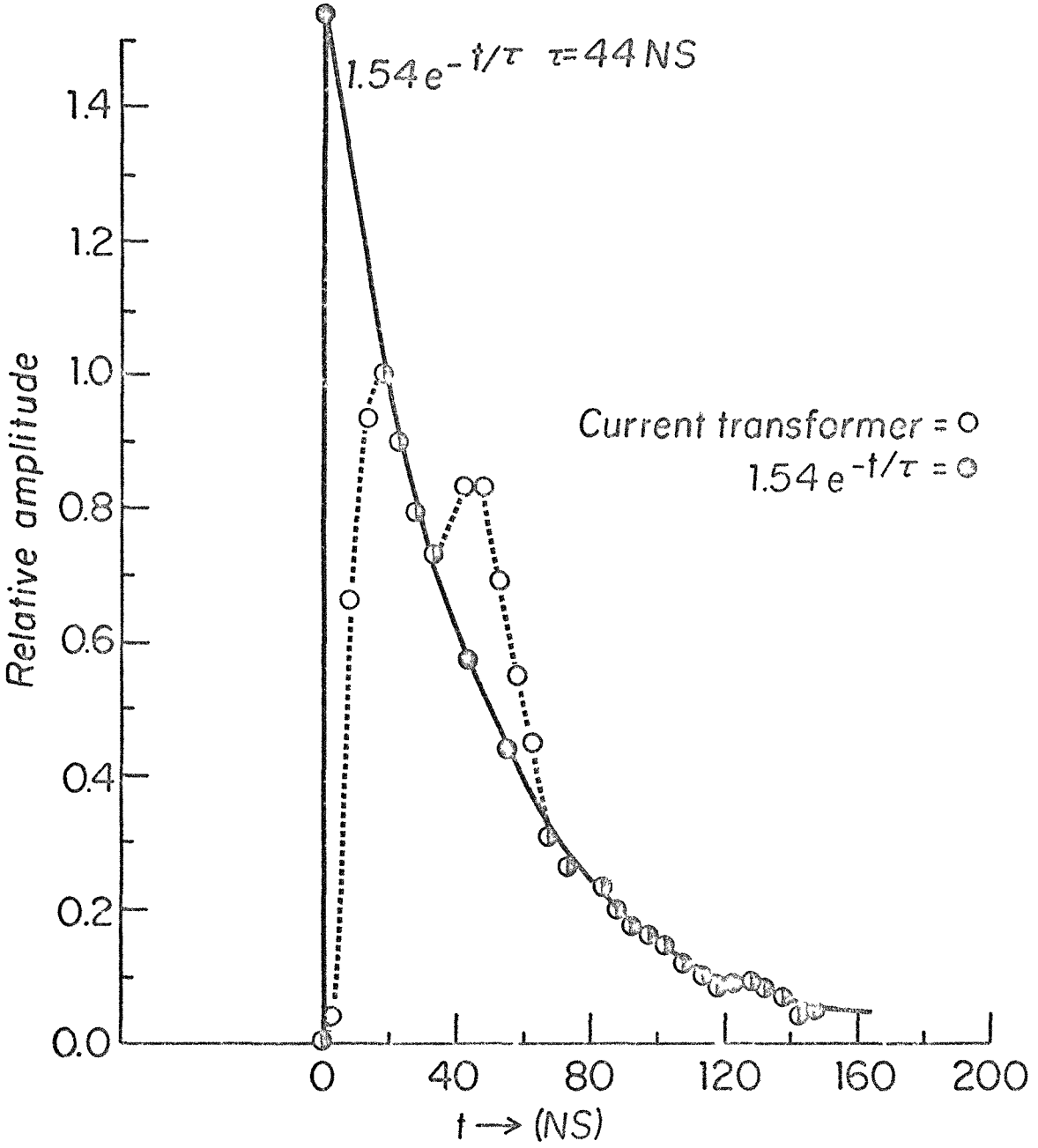
1.54 e^-t/τ τ=44 NS
Current transformer = O
1.54 e^-t/τ = O
Relative amplitude
1.4
1.2
1.0
0.8
0.6
0.4
0.2
0.0
0
40
80
120
160
200
t → (NS)

FIGURE VI

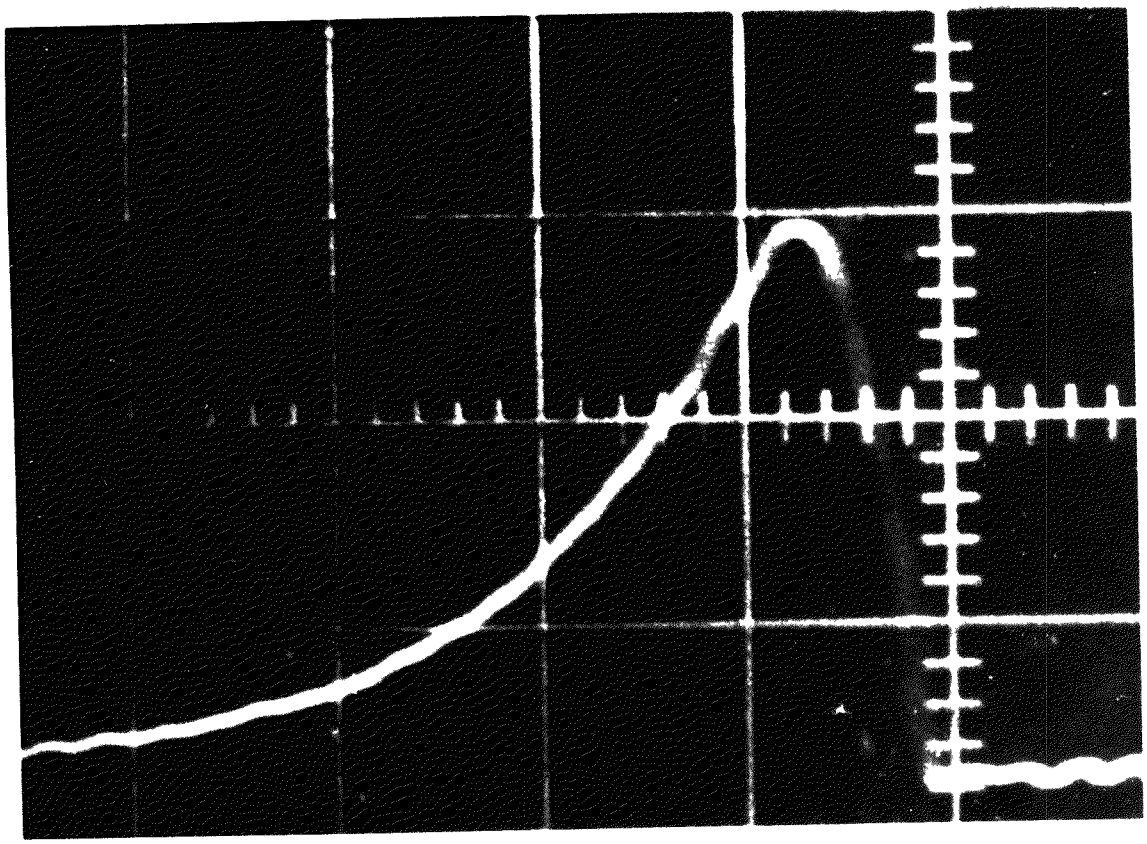

INTEGRATOR OUTPUT
100 NSEC/CM

Figure VII

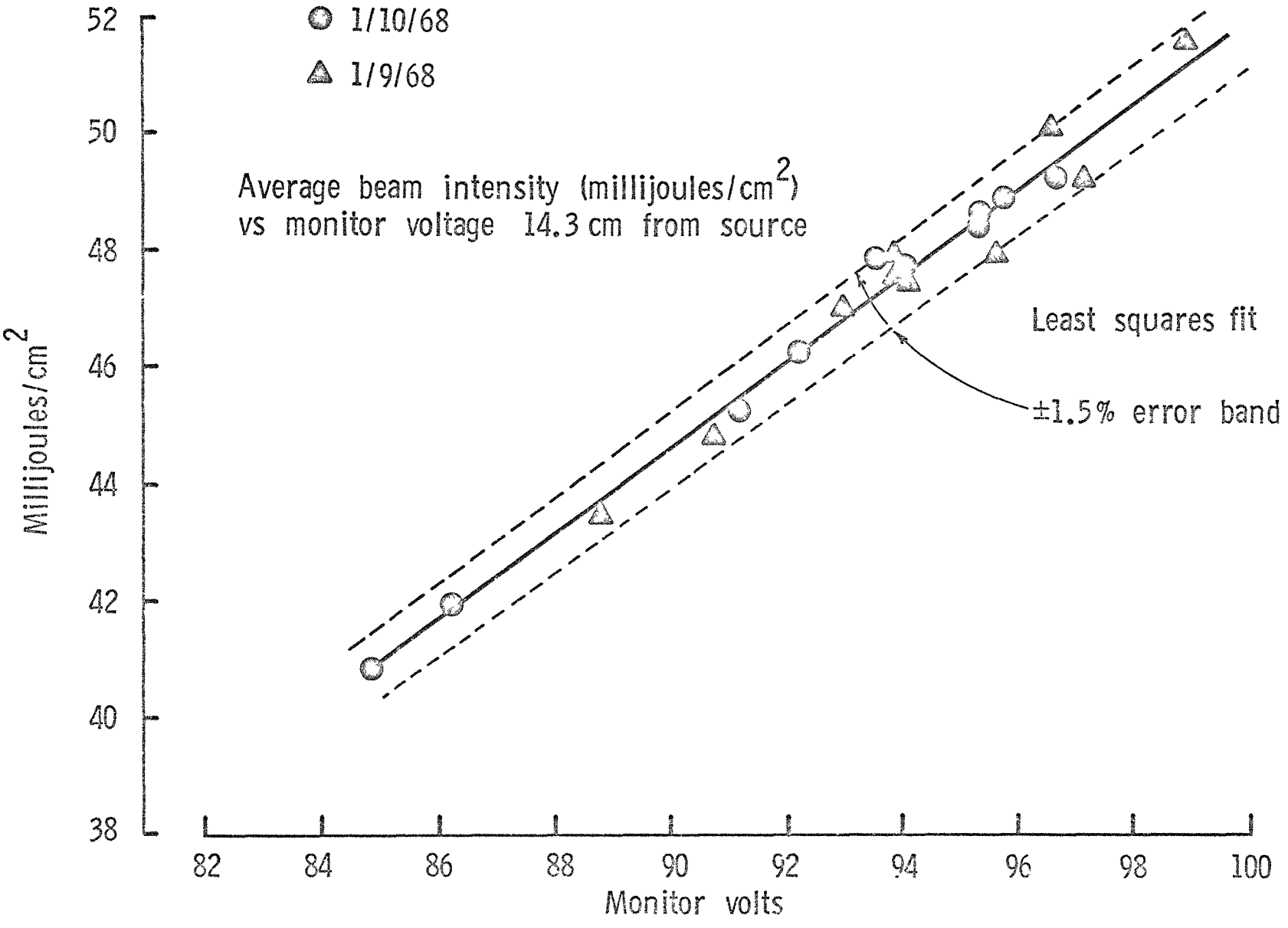
1/10/68
1/9/68
Average beam intensity (millijoules/cm^2)
vs monitor voltage 14.3 cm from source
Least squares fit
±1.5% error band
Millijoules/cm^2
52
50
48
46
44
42
40
38
82
84
86
88
90
92
94
96
98
100
Monitor volts

Figure VIII

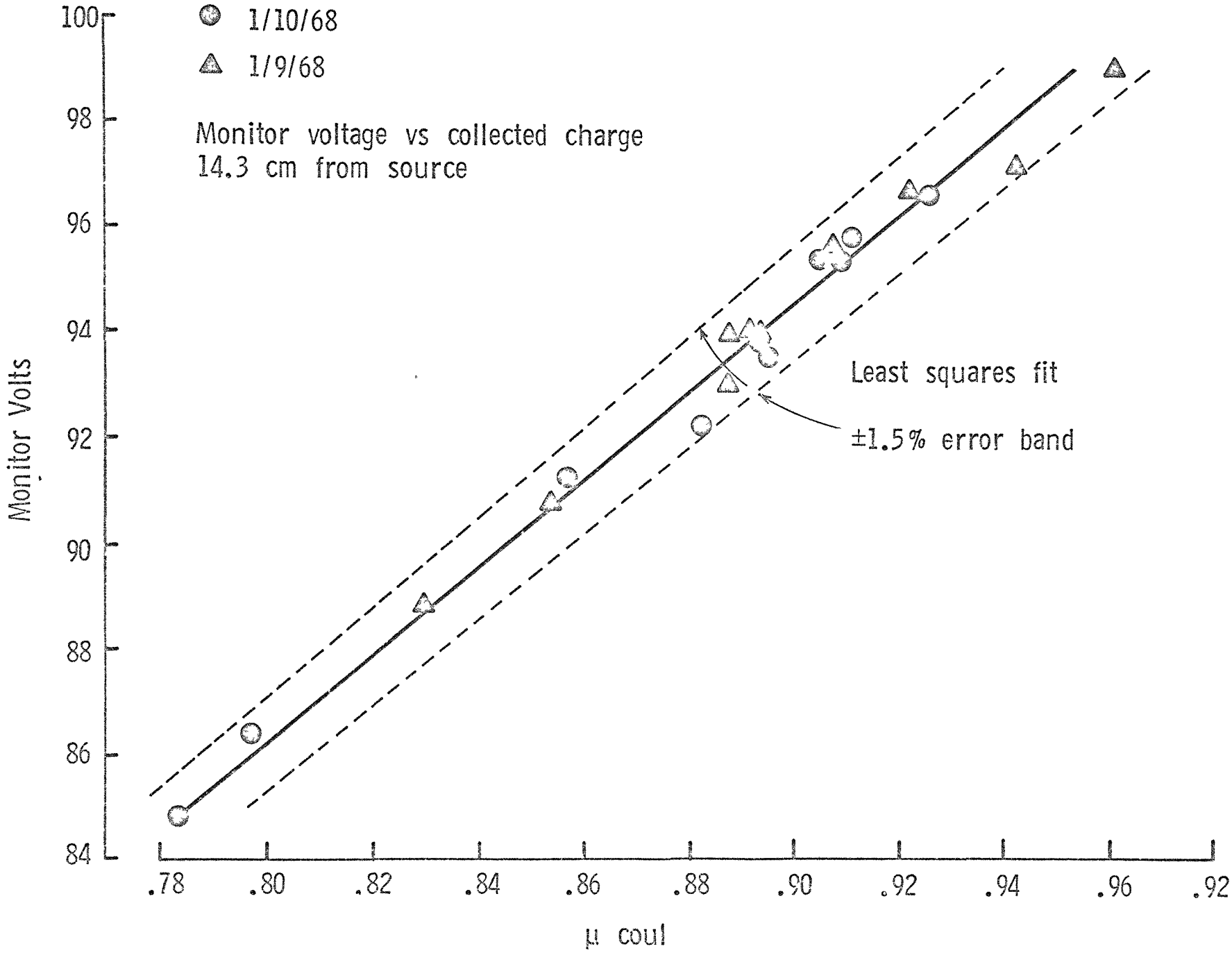
1/10/68
1/9/68
Monitor voltage vs collected charge
14.3 cm from source
Least squares fit
±1.5% error band
Monitor Volts
100
98
96
94
92
90
88
86
84
.78
.80
.82
.84
.86
.88
.90
.92
.94
.96
.92
μ coul

non linear relationship between coil output and energy or charge fluence is indicated. The functional nature of this non-linear relationship has not as yet been derived. While further investigations are in progress, it should be emphasized that the functioning of the monitor system is entirely satisfactory for normalization of biological and dosimetry experiments.

If the energy deposited per pulse and the collected charge per pulse are known, the average electron energy is determined. Average electron energies for various distances from the source are shown in Figure IX. The average electron energy was calculated at each distance as were the rms fluctuations. Root-mean-square fluctuations never exceeded ± 1.8%, and the average did not change significantly from day to day. The fall-off beyond 10.3 cm reasonably follows the approximately 2 KeV/cm slope expected for 500 KeV electrons in air.

It appears that most variations in source output are due to a change in the number of electrons emitted, since root-mean-square energy fluctuations are small (± 1.8%) compared to the total range of output variations (± 15%).

While short-term reproducibility of the monitor system as shown by the data presented is excellent; long-term changes in calibration occur. This difficulty arises from variations in sensitivity of the peak reading voltmeter. Periodic recalibration of the monitor is required until this problem can be overcome.

F. Energy and Charge Fluence

From the data obtained, we determined the manner in which intercepted energy or charge varies with distance from the source along the beam axis. This information is required since varying the source to target distance is the most convenient method of dose control for the field emission source. The variation of these quantities with distance for a typical electron source tube are shown in Figure X. Intercepted energy varies as $r^{-2.41}$ while charge varies as $r^{-2.39}$. Due to energy losses in the intervening air, the slope is slightly greater for the variation of energy with distance than for charge.

G. Thermoluminescent Dosimetry Studies

The performance of LiF and CaF_2:Mn thermoluminescent dosimeters has been studied over the dose rate region corresponding to the variation in beam intensity used in radiobiological experiments. Teflon matrix dosimeters 0.13 mm thick were affixed to the wafer in a dummy calorimeter to insure similar irradiation geometries. Nine dosimeters of each type were irradiated in groups of three at each of the selected distances and the corresponding distance functions computed by least squares analysis. Figure XI shows the normalized calorimetric and thermoluminescent distance functions. The tube used here was not the same one previously discussed, and consequently the calorimeter distance function is slightly different. The LiF and calorimetric distance functions are highly similar, while CaF_2:Mn shows a somewhat greater slope. Calculations based on fractional energy absorption by the dosimeters of the incident electrons give an estimated dose rate variation of from 1.5×10^{11} to 3×10^{12} rad/sec for the region investigated. Because of differences in diameter, the area covered

Figure IX

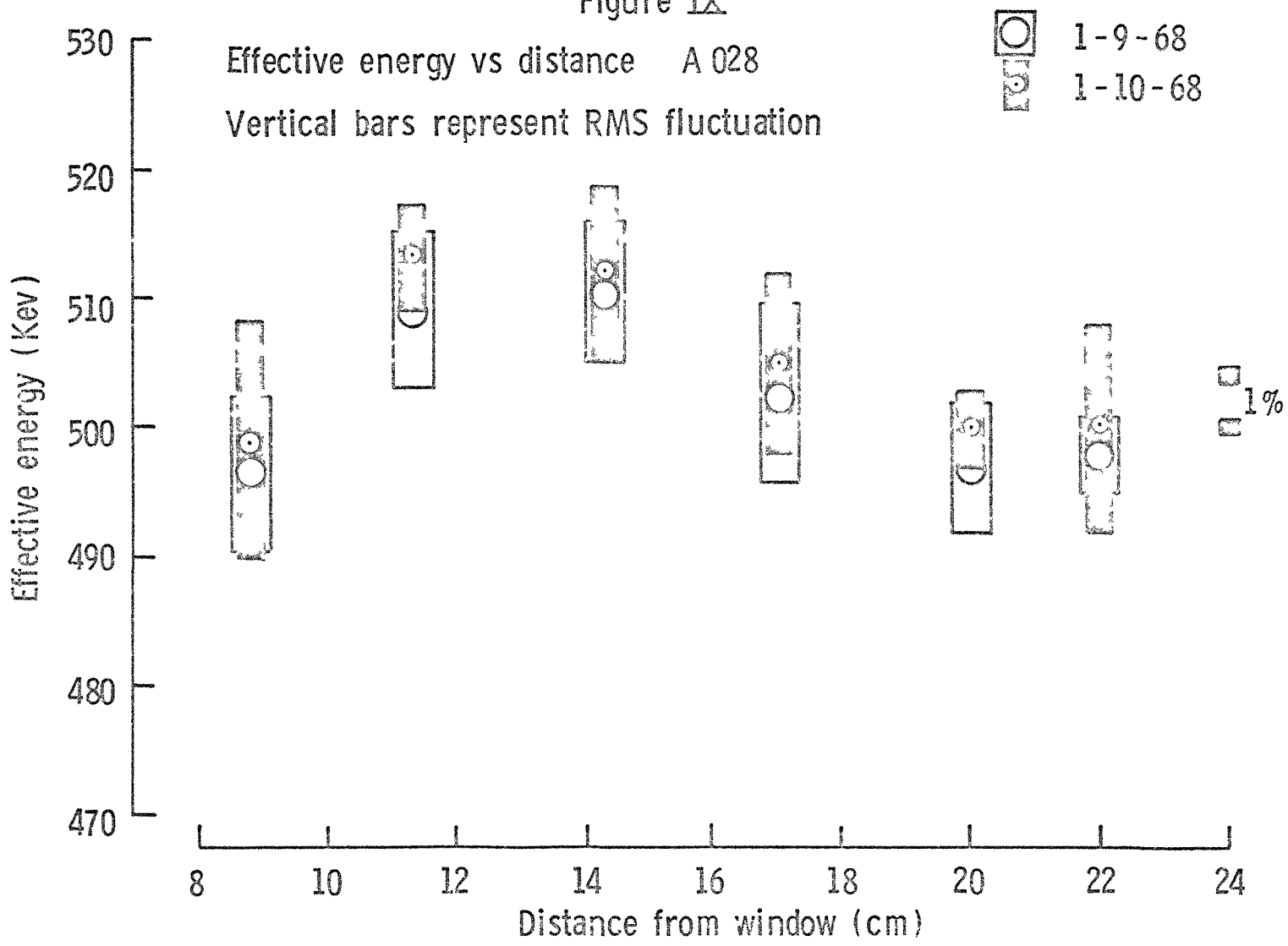
Effective energy vs distance A 028
Vertical bars represent RMS fluctuation
1-9-68
1-10-68
1%
Effective energy (Kev)
530
520
510
500
490
480
470
8
10
12
14
16
18
20
22
24
Distance from window (cm)

Figure X

LEAST SQUARES FIT
COLLECTED ENERGY VS DISTANCE
COLLECTED CHARGE VS DISTANCE

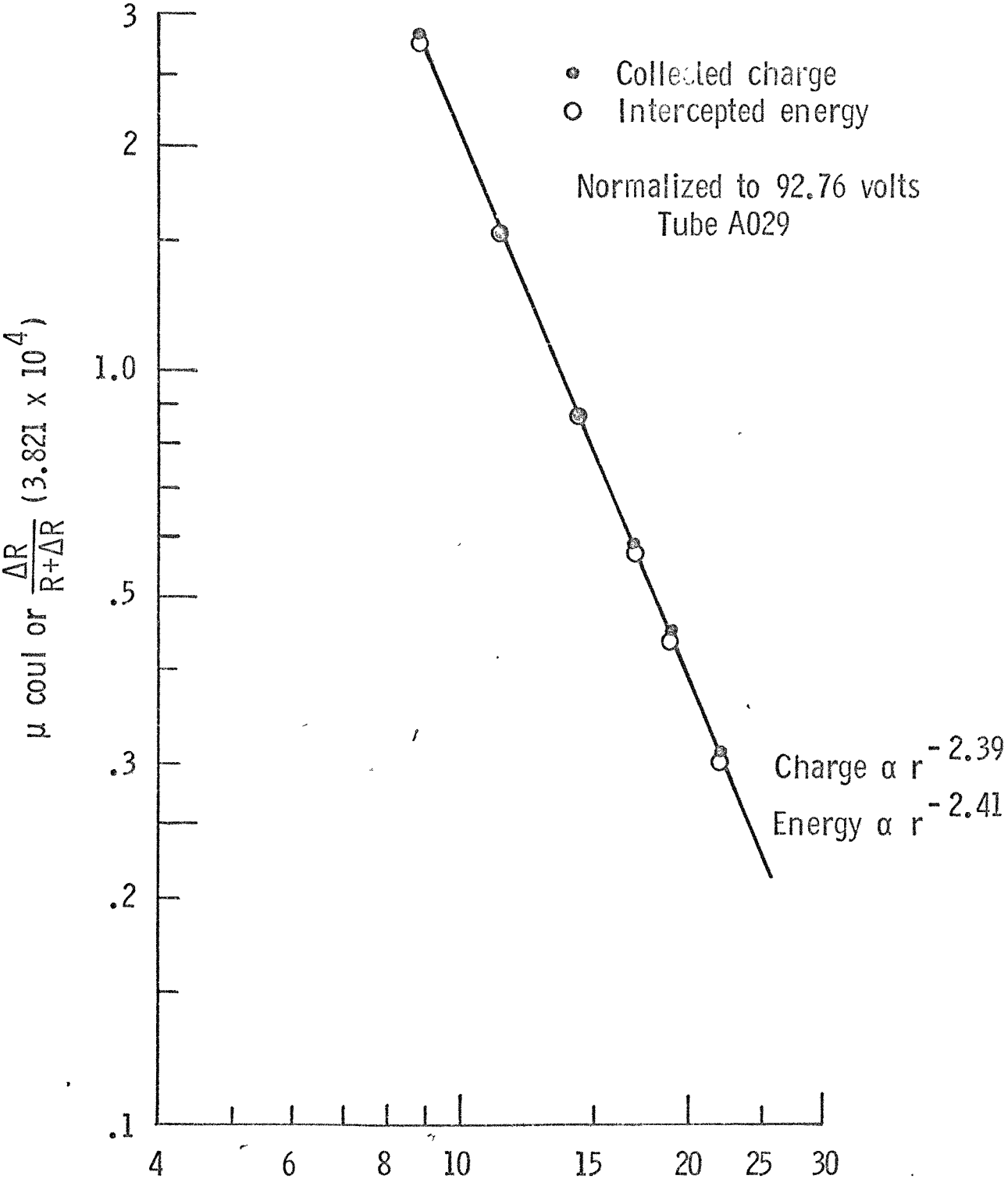

Figure XI

NORMALIZED CALORIMETER AND THERMOLUMINESCENT DOSIMETER RESPONSE VS DISTANCE FROM TUBE WINDOW CORRECTED TO EQUAL MONITOR READINGS

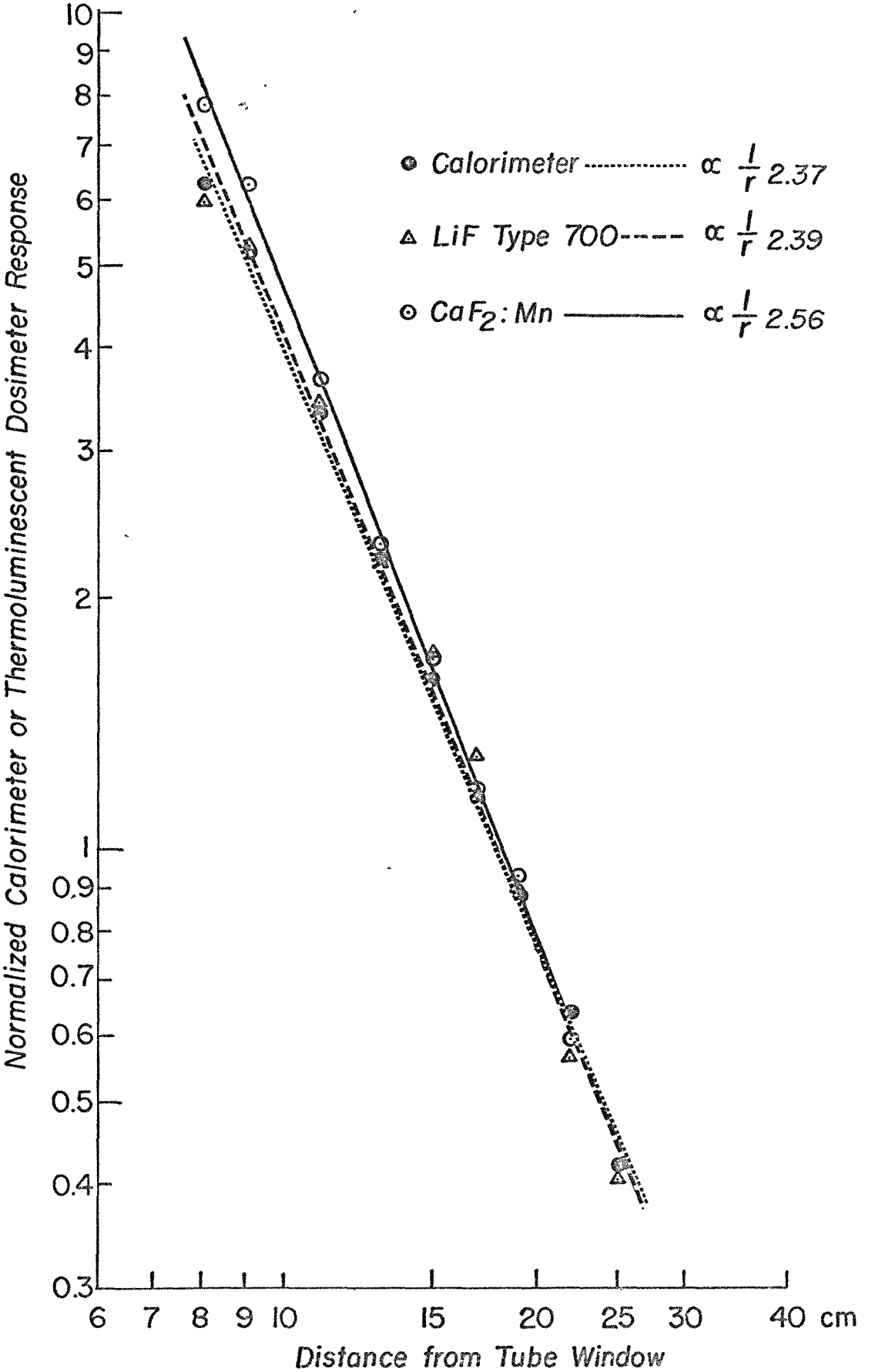

by the three CaF_2:Mn dosimeters was only about 10% of the area of the calorimeter wafer; while the LiF dosimeters covered about 40%. Therefore, the spatial distribution of energy on the dummy calorimeter wafer would probably influence the distance function obtained with the CaF_2:Mn dosimeters. To study the variation in field flatness, a number of irradiations with a total of twelve dosimeters affixed to the wafer were made at various distances. Typical results are shown in Figure XII. It is clear that the central area dose is 15% to 25% higher than the peripheral dose, and consequently the normalization of the CaF_2:Mn data based on average intensity was biased.

These preliminary experiments cover a limited dose-rate range and future work must extend this and correct for the known non-uniform spatial distribution. Results obtained to date indicate a lack of pronounced dose-rate dependence of the thermoluminescent materials and are very encouraging.

For the purpose of investigating the dose delivered to thin cell layers used in biological irradiations, the depth dose distribution has been examined using microtomed CaF_2:Mn teflon dosimeters. A depth dose distribution in polystyrene obtained with dosimeters from 15 to 30 microns thickness is shown in Figure XIII. The sets of dosimeters were exposed separately at each depth. While this minimized distortion of the depth dose distribution, it permitted fluctuations of dose in the plane perpendicular to the beam direction to affect the accuracy of the measurements. The experimental points were fitted to a fourth degree polynomial by least square analysis. This fit indicates a surface dose of approximately 67% of that at the dose maximum. The extrapolated range of 173 mg/cm^2 is slightly less than the 178 mg/cm^2 calculated for monoenergetic 500 KeV electrons in polystyrene.

H. Preliminary Experience with 3 Nanosecond Pulse Source

The 2 Channel 706 Field Emission Corporation pulsed electron source produces a beam of about 4000 amperes in 3 nsec for each channel. Two tubes are available and have been used in the preliminary studies; the 5515 and 5510 tubes. The field emission emitters are more closely spaced in the 5515 tube and produce a higher current density beam than in the 5510 tube. In both tubes, the electron beam exists through a .075 mm titanium window.

In such high current density electron beams, a phenomenon occurs which is known as the Bennett "Pinch." The effect is due to ionization of the air by the electron beam where the secondary electrons migrate out, and a net positive charge causes a magnetic refocusing of the diverging primary electron beam. The "Pinch" effect is greater for the 5515 tube, since the current density is larger. According to data provided by Field Emission Corporation, the energy fluence in air measured as a function of distance from the tube window should display a plateau for the first 10 cm and then fall off as $r^{-2.5}$. With a 0.012 mm tungsten scatterer at the window, the energy fluence in air should immediately fall off with little plateau, and the same is true with the beam in vacuum. In the case of the scatterer placed in front of the window, the absence of the pinch, as exhibited by the lack of plateau is due to the smaller current density. In vacuum, there is no air to ionize, consequently, no pinch can be produced. Maximum pinch occurs at about 100 microns pressure.

Figure XII

TYPICAL % DOSE DISTRIBUTIONS ON CALORIMETER WAFER AT VARIOUS DISTANCES FROM SOURCE

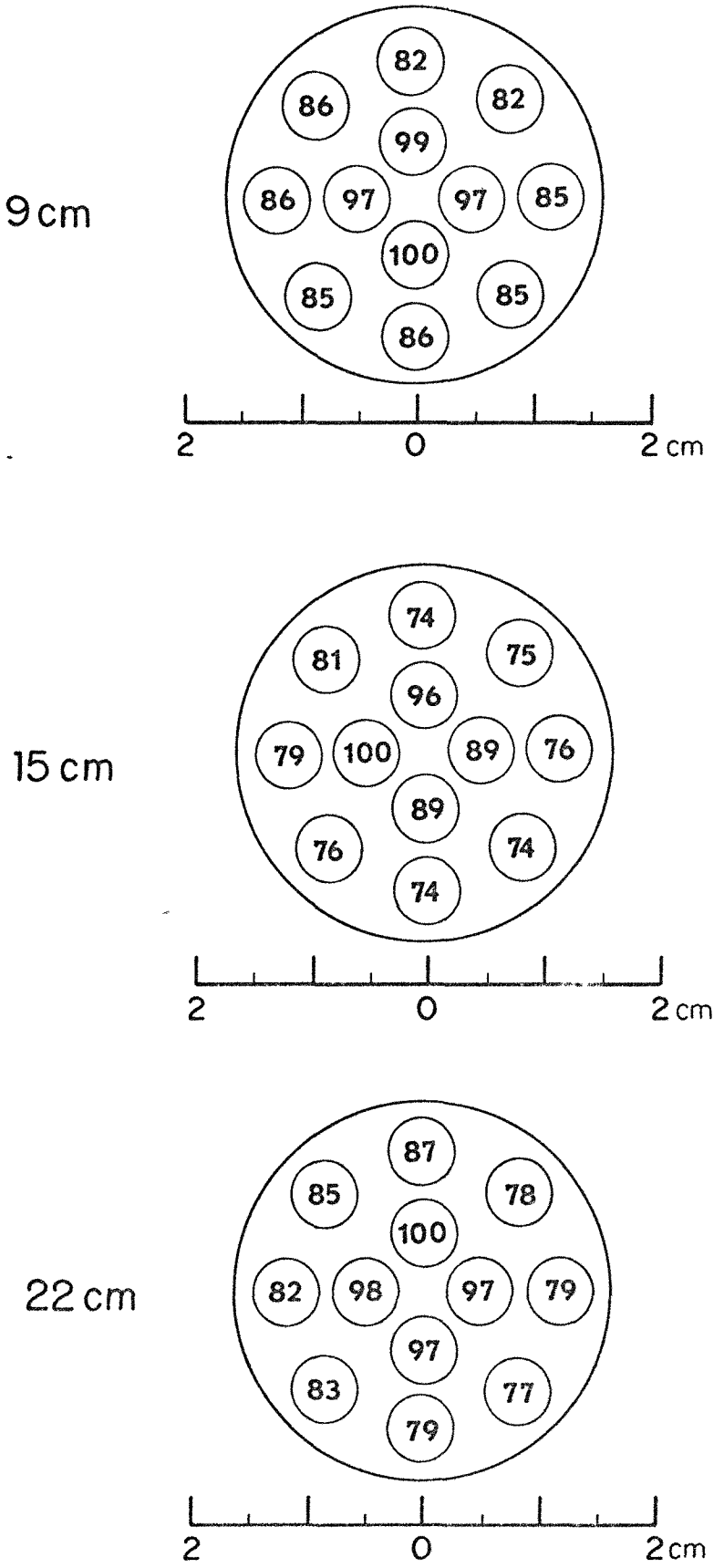

Figure XIII

DEPTH DOSE IN POLYSTYRENE FIELD EMISSION ELECTRON SOURCE

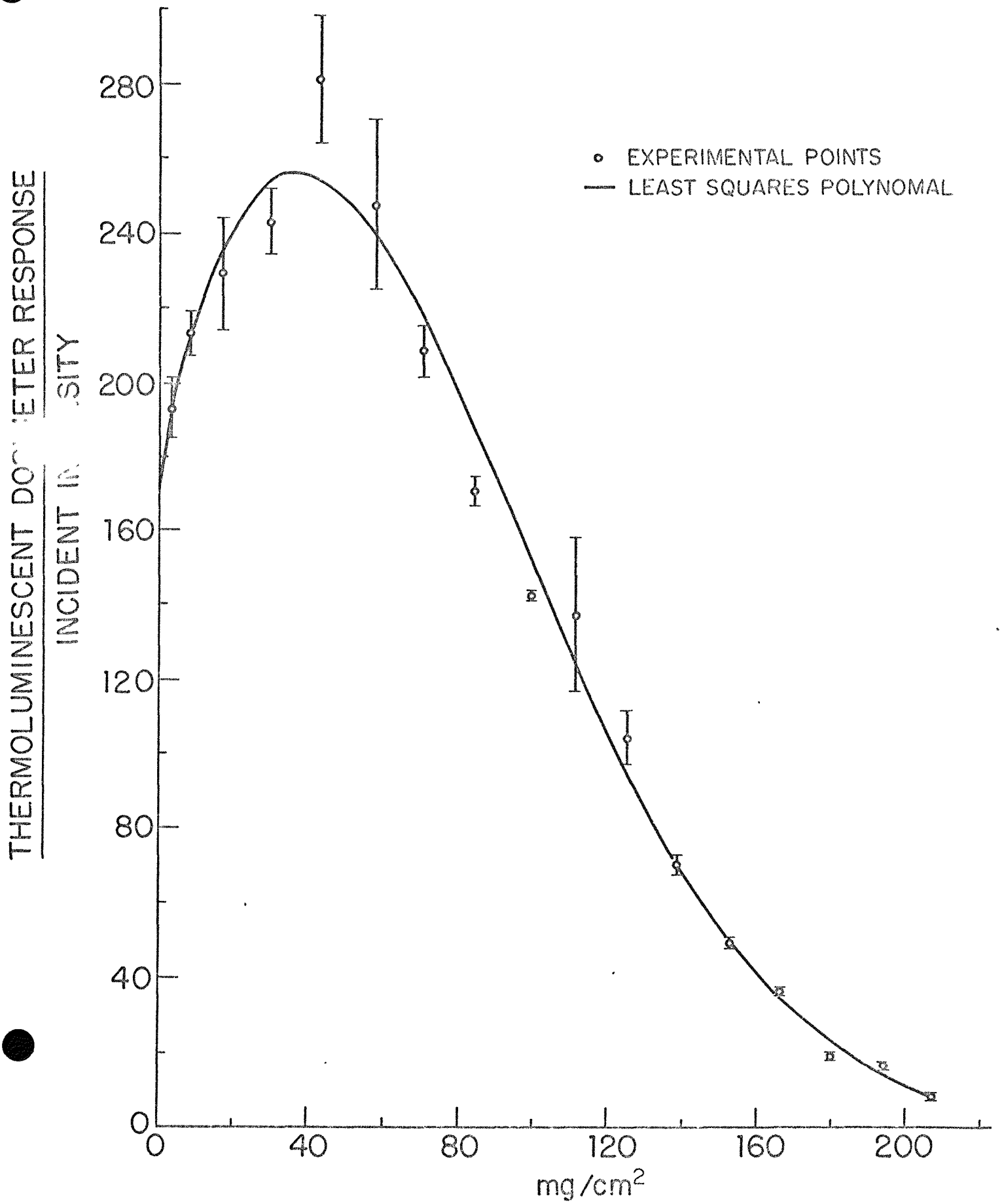

Energy density as a function of distance was measured here with the calorimeter for the cases of: no scatterer; 0.25 mm tungsten scatterer; and vacuum. In air, the existence of the plateau and power law fall-off were demonstrated. However, in our experiments, the pinch was not eliminated by the use of a scatterer. When measurements were performed in air, pulse to pulse repeatability was poor, with frequent variations of ± 20% occurring. Since these large fluctuations were not observed with the calorimeter close to the window, it was felt that the pinch was not stable and consequently produced shifting of the beam and changes in intercepted energy. In an attempt to improve the situation, the beam was surrounded with a coaxial conductor. This produced an increase of an order of magnitude in the energy measured by the calorimeter and a slight improvement in reproducibility. In order to avoid entirely the problems caused by the pinch, adjustable length vacuum columns fitted with either 0.037 mm titanium or 0.05 mm mylar windows were constructed. Initial experiments have been performed with the calorimeter attached to these columns. Improved repeatability and a power law fall-off in dose are observed.

The results with the vacuum columns are quite preliminary but indicate the necessary conditions for further investigation in the use of these extremely short pulse electron sources. These are that the beam must go into vacuum to eliminate the Bennett Pinch, the geometry should be coaxial, with the electrons returned immediately back to the machine by solid conductors.

III. INTERLABORATORY INTERCOMPARISON

A. Introduction

During the report period, this laboratory has been engaged both as a consultant and participant in the National Bureau of Standards (NBS) electron dosimetry uniformity study. A brief report of our consultation activities and a discussion of our experience as a participant in this study are given below.

The NBS electron dosimetry study is carried out by shipment of standard quartz cells containing Fricke dosimeter solution to participating institutions. These are irradiated according to the AAPM protocol (8) with high energy electrons. The exposed dosimeters together with the participants' estimates of the doses delivered are returned to the NBS, where the dosimeters are read and the doses, corrected for any observed shift in unexposed control dosimeters, are calculated. A comparison of the dose as estimated by the participants and the dose as computed by the NBS is made. The tabulated results for all institutions, together with identification pertinent to the individual institution, are then returned to each participant.

B. Consultation

This laboratory's activities as a consultant during the report period covered two areas. The first was the comparison of the yield of Fricke dosimeter solution prepared by the NBS with that prepared at Sloan-Kettering Institute (SKI). The second was the investigation of the effect of irradiating the dosimeter solution in the standard quartz cells compared with irradiation directly in a cavity in the phantom material.

Table I compares the yield of three separate preparations of dosimeter solution from NBS with preparations by this Institute for ^{60}Co gamma-rays and several energies of electrons. Irradiations were performed in similar quartz cells in the AAPM polystyrene phantoms.

TABLE I

Ratio of Yield of NBS/SKI Fricke Dosimeter

	PREPARATION		
Radiation	A	B	C
^{60}Co Gamma	0.997 ± .004	0.984 ± .006	1.01 ± .015
6 MeV Electrons	---	---	1.04 ± .02
10 MeV Electrons	1.002 ± .005	---	---

The results, with the exception of the 6 MeV data, are satisfactory as they indicate that the characteristics of the dosimeter are uniform from solution to solution even when prepared by different laboratories. A possible explanation for the 6 MeV ratio exceeding unity by 4 per cent, may be the presence of air bubbles in the NBS cells. These bubbles might have perturbed the dose distrubution noticeably for the low energy electrons. This possibility will be studied subsequently.

The response of Fricke dosimeters for various radiations when irradiated in quartz cells compared with those irradiated directly in polystyrene is shown in Table II:

TABLE II

Comparison of Response of Fricke Dosimeters
Irradiated in Phantom

Radiation	Ratio $\frac{\text{Quartz Cells}}{\text{Polystyrene Cells}}$
^{60}Co Gamma-Rays	1.010 ± .004
6 MeV Electrons	1.014 ± .019
15 MeV Electrons	0.981 ± .019
20 MeV Electrons	0.995 ± 0.010

These results support our previous conclusion (9) that the use of quartz cells did not seriously perturb the dose measured in the medium at the reference depths (1.5 cm for 15 and 20 MeV electrons and ^{60}Co gamma-rays, 1.0 cm for 6 MeV electrons).

C. Participation of NBS Electron Dosimetry Uniformity Check

From July 1967 to May 1968, this laboratory has participated in the four dosimetry uniformity checks undertaken by the NBS. The results of these checks are summarized in Table III and will be discussed following a description of the procedures employed. Prior to the scheduled check, Fricke dosimeter calibrations of the betatron were made. These calibrations consisted in the exposure of dosimeters in cells identical to those of the NBS at the chosen energies. Dose was calculated assuming a GFe^{+++} of 15.5† and using an extinction coefficient of 2.2×10^3 as measured for our spectrophotometer. Average standard deviations of ± 1.5% were observed, this is about 0.5% greater than found when the dosimeters are exposed in polystyrene cells. The difference is possibly due to the presence of a small air space surrounding the neck of the quartz cells when placed in the phantom.

A total of eight cells was received from the NBS for each check. Of these, two served as controls and two were irradiated at each of three energies. The estimated fractional error in the dose delivered to the NBS cells based on the average deviations of cells readings and uncertainty in the extinction coefficient was ± 1.8%. Allowing for a similar uncertainty in the NBS determination of dose, the ratio of the dose estimated by this laboratory to that reported should be within ± 2.6% of unity.

TABLE III

Ratio of SKI Estimated Dose to NBS Reported Dose Intercomparison

Electron Energy	July 1967	Nov. 1967	Jan. 1968	May 1968
6 MeV	*	1.067	1.000	1.057
10 MeV	*	1.033	--	--
15 MeV	-	--	0.989	1.014
20 MeV	*	1.037	1.022	1.024

*Test results considered to be valid by NBS due to faulty preparation of their irradiation cells.

†(The same used by the NBS.)

With the exception of two of the 6 MeV comparisons, the results are what might be expected granting the inherent limitations of the experiment. However, the problem of insuring uniform dosimetry of high energy radiations still requires continued attention.

IV. NEUTRON DOSIMETRY

Because of the potentially greater efficacy in cancer radiotherapy of neutrons based on lower oxygen enhancement ratios (10), considerable research with them has recently been undertaken (11,12,13). The acquisition by the Institute of a 30 inch cyclotron provides a source capable of producing a wide variety of neutron spectra with maximum energies from 5.5 MeV [Ni^{58} (p, n) Cu^{58}] to 28.5 MeV [Be^{9} (He^{3}, n) C^{11}]. The estimated dose rate in tissue at 100 cm from the target, based on available beam currents, is from 5 to 80 rad/min, depending on the reaction chosen. Since it is desired to conduct biological investigations using this source, a program to provide dosimetry information has been initiated.

To provide preliminary information on total tissue dose and spatial distribution, an ionization chamber has been constructed from Shonka tissue equivalent conducting plastic. This chamber, together with a large phantom contain tissue equivalent liquid and a remote positioning device (14), is shown in Figure XIV. The chamber is of the pancake type with a collecting volume 2 cm in diameter and 0.2 cm thick. This geometry was chosen since it facilitates comparison with chemical or calorimetric standards.

V. SOLID STATE DETECTOR EVALUATION

A. Two-Dimensional Matrix of Lithium Drifted Diodes

This application was proposed (AEC Proposal 1966 and 1967) as being pertinent to the use of isotopes in biological and clinical investigations. Specifically, it is aimed toward providing a means for mapping the intensity distribution of extended isotopic sources more quickly and accurately than is otherwise readily available. Applications to isotopic uptake studies in human tissue were envisioned. Although operational characteristics of such devices are still under investigation, data obtained during the period of this report indicate the applicability of the proposed device geometry in obtaining particle position information with a lithium drifted diode. As described in a previous report (15), the geometry is based upon the formation of individual detection regions on a single bulk diode through the use of high resistance grooves which define orthogonal, electrically isolated electrodes between the p and n regions (Figure XV). This permits a row-column method of addressing charge pulses liberated by absorbed particles and also admits the practicality of assembling such devices into larger arrays. For arrays of significant size, this configuration results in a marked reduction in the number of data channels required for "read-out" compared to the alternative approach of a "checkerboard" type of partitioning which requires one data channel per detection region.

FIGURE XIV

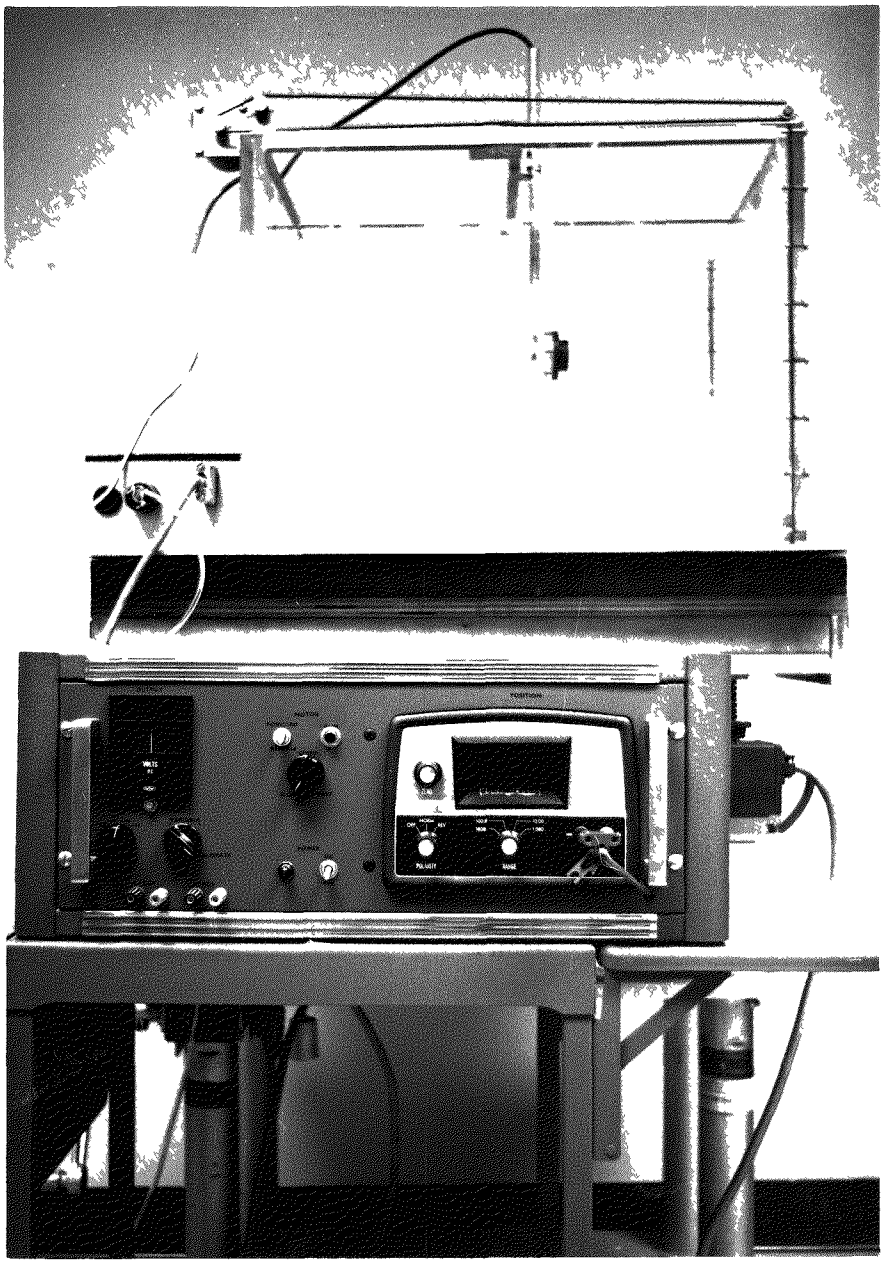

NEUTRON ION CHAMBER IN PHANTOM WITH
POSITIONING MECHANISM

Figure XV

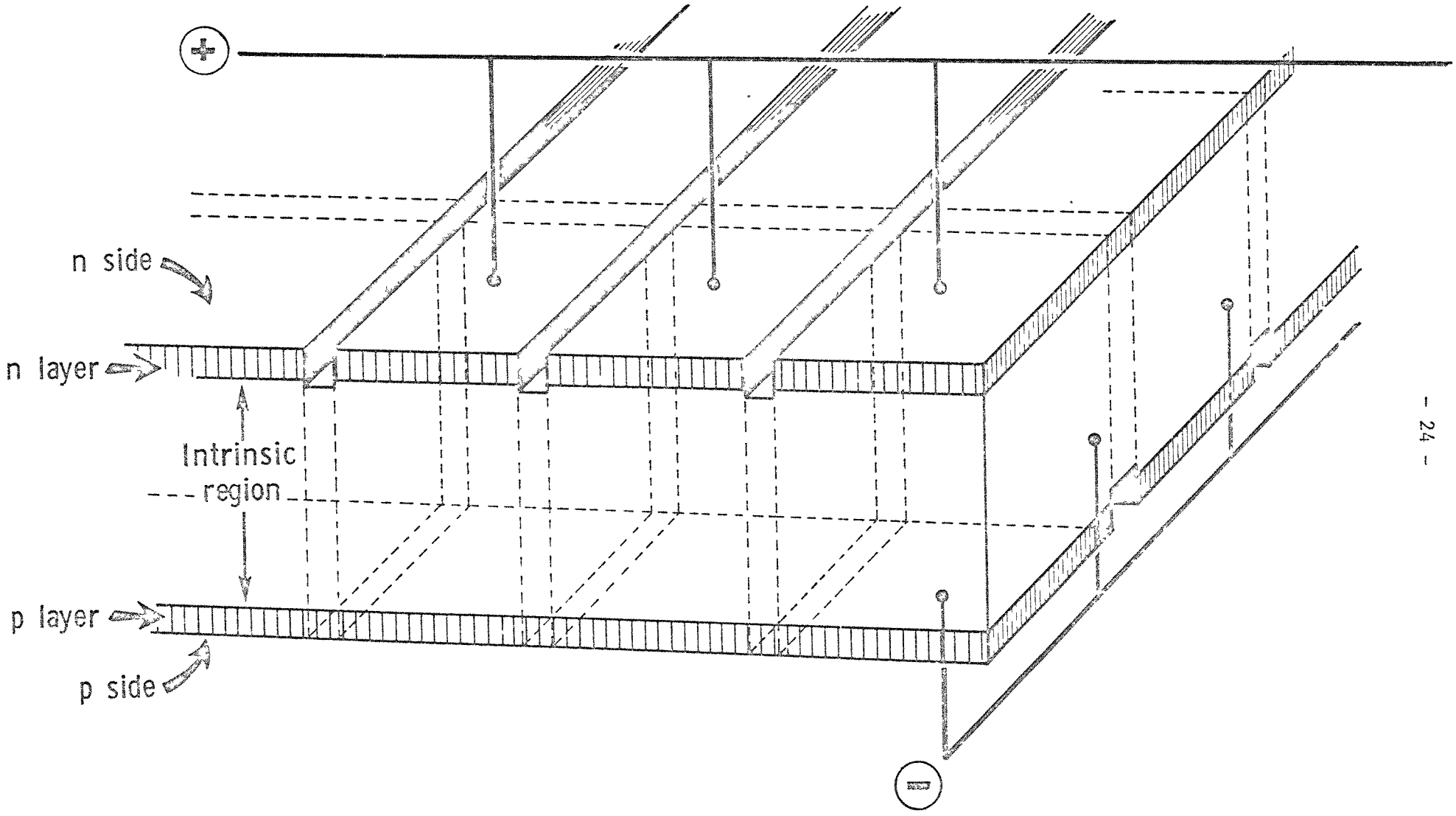

OF ONAL ELECTRODE STRIP MATRIX

1. Matrix structure and fabrication

The matrix whose properties will be described in detail is shown in a test jig in Figure XVI. Above the matrix, a radioactive source holder is in position to indicate operating geometry. The use of ultrasonic bonding techniques to attach lead wires to subsequent units will significantly streamline the arrangement. This will be discussed further below. The fabrication of this matrix was newly completed at the end of the last report period. For convenience of reference, its structure and fabrication are recapitulated here.

A 25 mm diameter, 4 mm thick cylindrical wafer of float-zone p type (250-300) ohm-cm silicon was lithium drifted to a depth of 3 mm using the constant wattage method of Miller et al. (16). Lithium drift depth was verified by the usual copper staining techniques. Following the drift, the device was cut into a 1.6 cm square. Using a diamond wheel with a grinding machine, 5 parallel grooves .5 mm wide were cut into each face of the diode, those on the n side laying at right angles to those on the p side. Six separate electrode strips 2.2 mm wide were thus formed on each side. Etch removal of the damage was followed by a suitable number of deionized water rinses.

2. Matrix electrical characteristics

Inter-electrode strip resistance, reverse leakage current, and noise levels (FWHM) associated with the individual strips were measured. High groove resistance is needed to obtain adequate operational isolation between electrode strips. Groove resistance also has a bearing on the electric field distribution at the boundaries of separate detection regions and will have a major influence on ultimate spatial resolution. On the other hand, noise levels, depending partly on leakage current levels, determine minimum detectable particle energies; that is, signal levels, and how many such devices can be effectively joined together in a larger assembly.

a) Noise levels of individual electrode strips

1. Experimental arrangement

In order for the noise measurements (FWHM) to reflect operational characteristics of the matrix, each electrode strip on both n and p sides was measured while reverse bias was applied across the entire matrix. This was to allow for the possibility of noise injection from neighboring strips under operational conditions. As is usual, these measurements were performed with a charge sensitive preamplifier (f.e.t. input) and a main pulse shaping amplifier. Double differentiation and single integration time constants were set at .2 μs. FWHM values were obtained by conversion of an r.m.s. volt meter's readings at the main amplifier output. During these measurements, the matrix was in ambient of pure (99.97%) dry (dew point - 88°F) flowing nitrogen at a reproduced flow rate and for a sufficient time to ensure equilibrium conditions.

Figure XVI

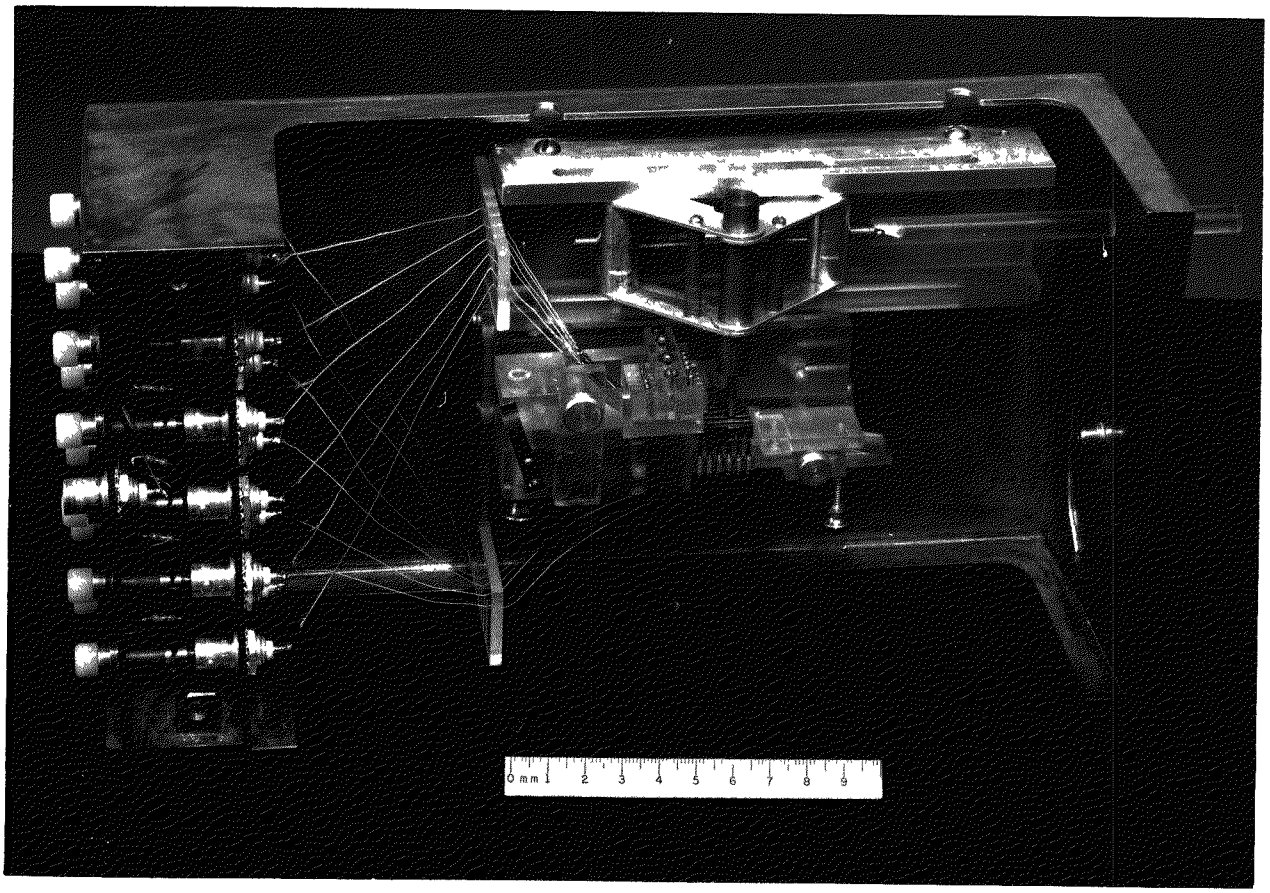

Matrix in Test Jig

2. Results

Noise levels, (FWHM), versus reverse bias for the n side electrode strips are shown in Figure XVII. The upper curve represents the noise level for all strips in parallel. As is expected, similar data are obtained from measurement of the p side strips. This is shown in Figure XVIII.

b) Groove resistance of p and n side of matrix

1. Experimental arrangement

By resistance values of the matrix grooves is meant the slope ($\Delta V/\Delta I$) of the measured current versus voltage characteristic of the grooves on the n and p side. Where the curves are nearly linear, the average slope is valid. Where near linearity is not the case, the lowest value is considered applicable. Throughout these measurements, attempts were made to reproduce clean, dry ambient conditions. The measurements were made with the equipmental arrangement indicated on the left side of Figure XIX. The matrix was under a range of reverse biases during measurements of the current-voltage characteristics across each groove. The use of the internal nulling circuit of a pair of Keithley micro-volt-ammeters made it possible to measure only the current change across the groove; that is, the reading of the leakage current to the opposing diode face was "bucked out" before voltage was applied across the groove. The current meters indicated in the schematic were in place simultaneously only during the initial series of measurements. Subsequently, the current to the left and right of the electrode strip at which the voltage was applied was measured in tandem.

2. Results

Figure XIX shows the current voltage characteristics of the grooves on the n side of the diode with a fixed 200 volts reverse bias across the matrix. The inverse slope of the upper curves indicates groove resistances well over 10^9 ohms for all grooves. Figure XX shows the current-voltage characteristics of a single representative groove for a number of bias voltages. The groove resistance level is not appreciably different over the range of bias voltage, remaining in excess of 10^9 ohms for biases over 200 volts. These values are comparable to those obtained by Hayashi *et al.* (17) for a pair of annular n side grooves of a detector telescope assembly. Leakage current versus bias curves for each strip are shown at the bottom of Figure XIX. The curve marked total I-V represents the measurement for strips in parallel.

3. Degeneration of p side groove resistance

Initial p side groove resistance values were comparable to those on the n side. However, it was observed that for this unpassivated device, in contrast to the n side, a deterioration of p side groove resistance takes place due to ambient effects on the surface. This can be seen in Figure XXI which shows current voltage curves for the p side grooves at 500 volts bias. This indicates that all grooves (with the exception of that associated with the sharply upturned curve) have resistances of around only 5×10^7 ohms. It is known that this deterioration can be retarded from data obtained from an

Figure XVII

MATRIX OS-2

NOISE MEASUREMENTS OF INDIVIDUAL n-SIDE ELECTRODE STRIPS VS REVERSE BIAS

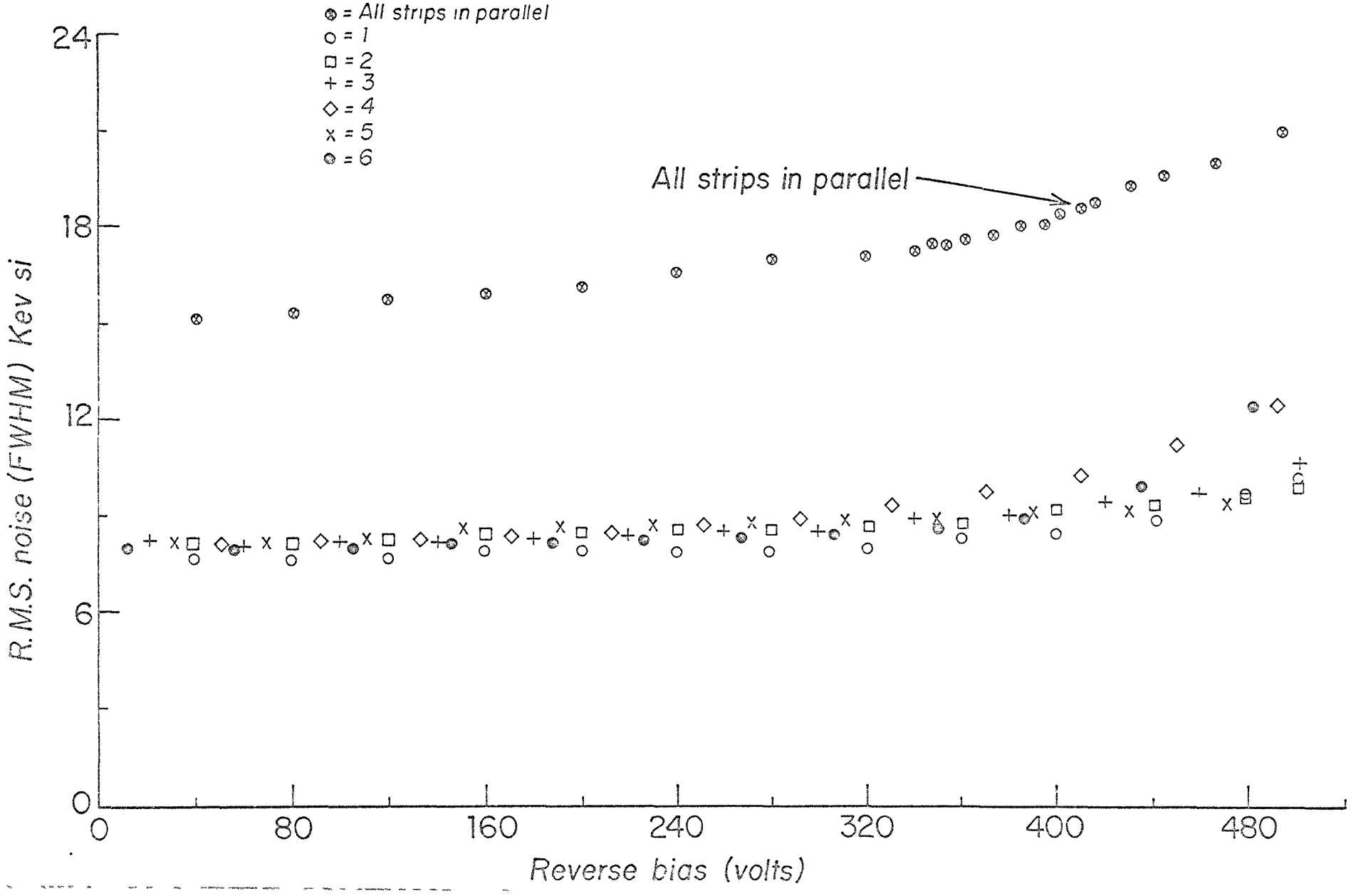

Figure XVIII

MATRIX OS-2

NOISE MEASUREMENT FOR INDIVIDUAL P-SIDE ELECTRODE STRIPS VS REVERSE BIAS

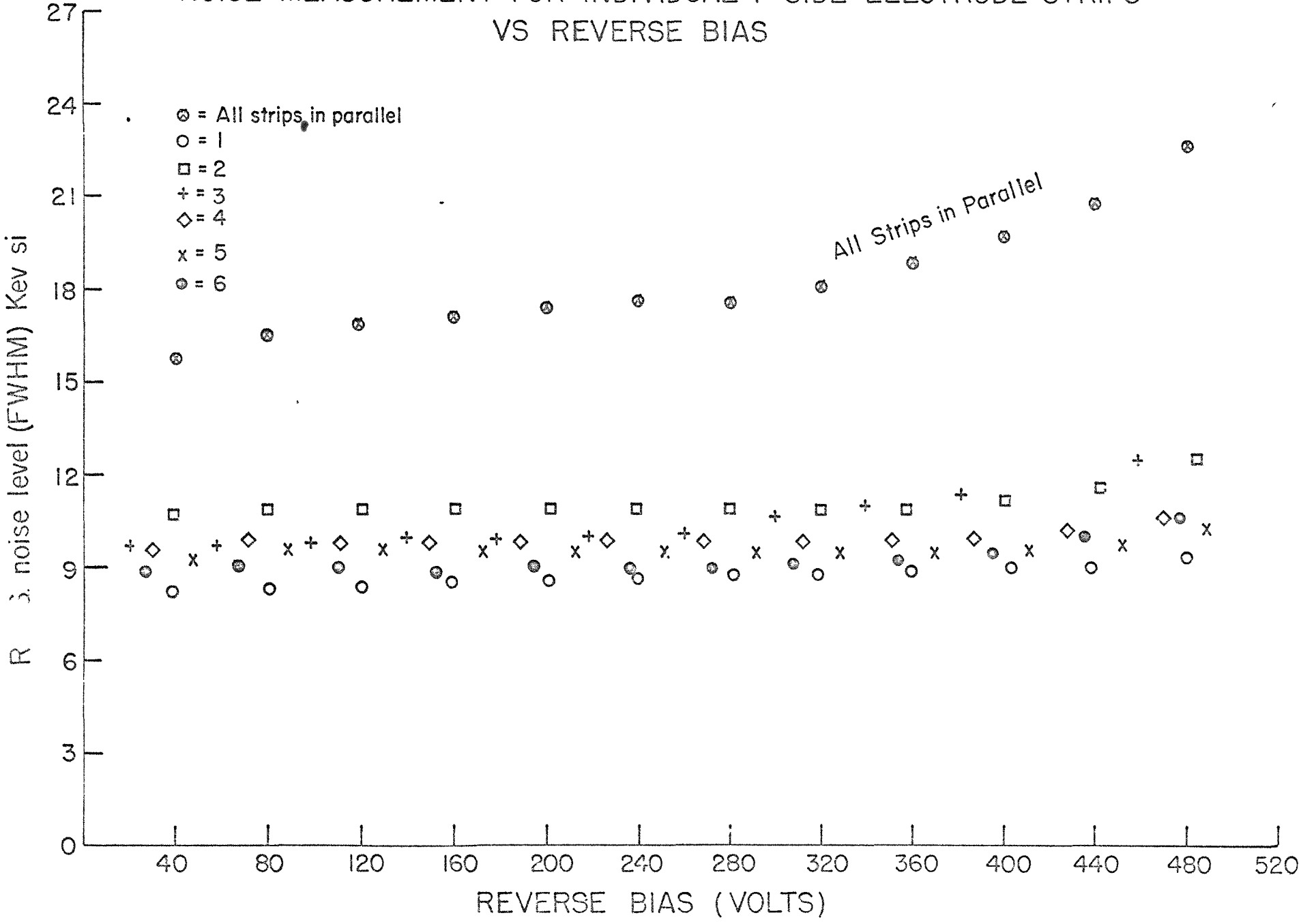

Room temp.
19°C

Ambient in test box
N_2 (~2.5 cfh)

Figure XIX

MATRIX OS-2

CURRENT-VOLTAGE CHARACTERISTIC ACROSS n-SIDE GROOVES FOR 200 VOLTS REVERSE BIAS (TOP)
REVERSE CURRENT-VOLTAGE CHARACTERISTIC OF n-SIDE STRIPS SINGLY AND IN PARALLEL (BOTTOM)

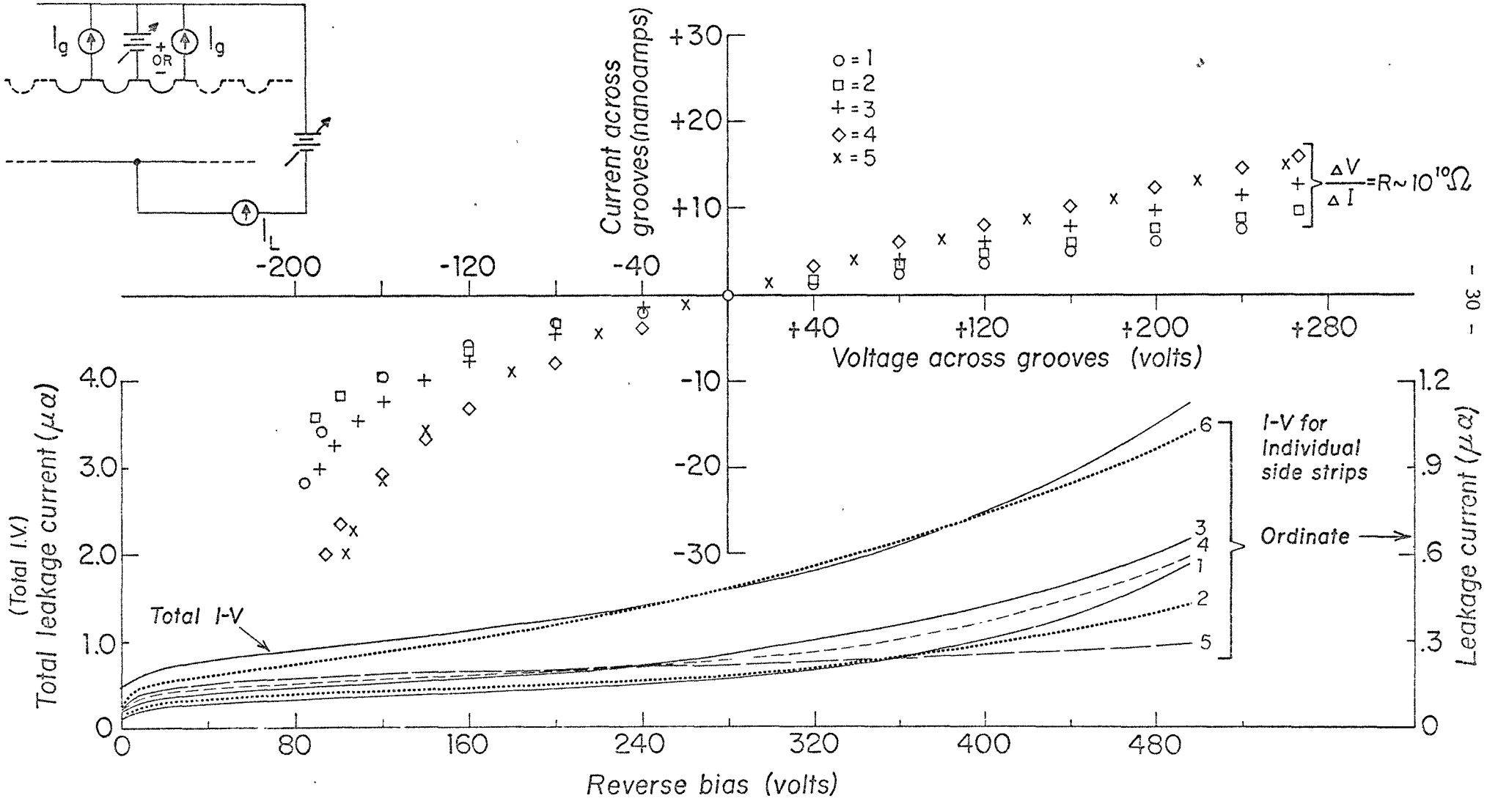

Figure XX

MATRIX OS-2

CURRENT VOLTAGE CHARACTERISTIC ACROSS ONE n-SIDE GROOVE AT DIFFERENT REVERSE BIASES

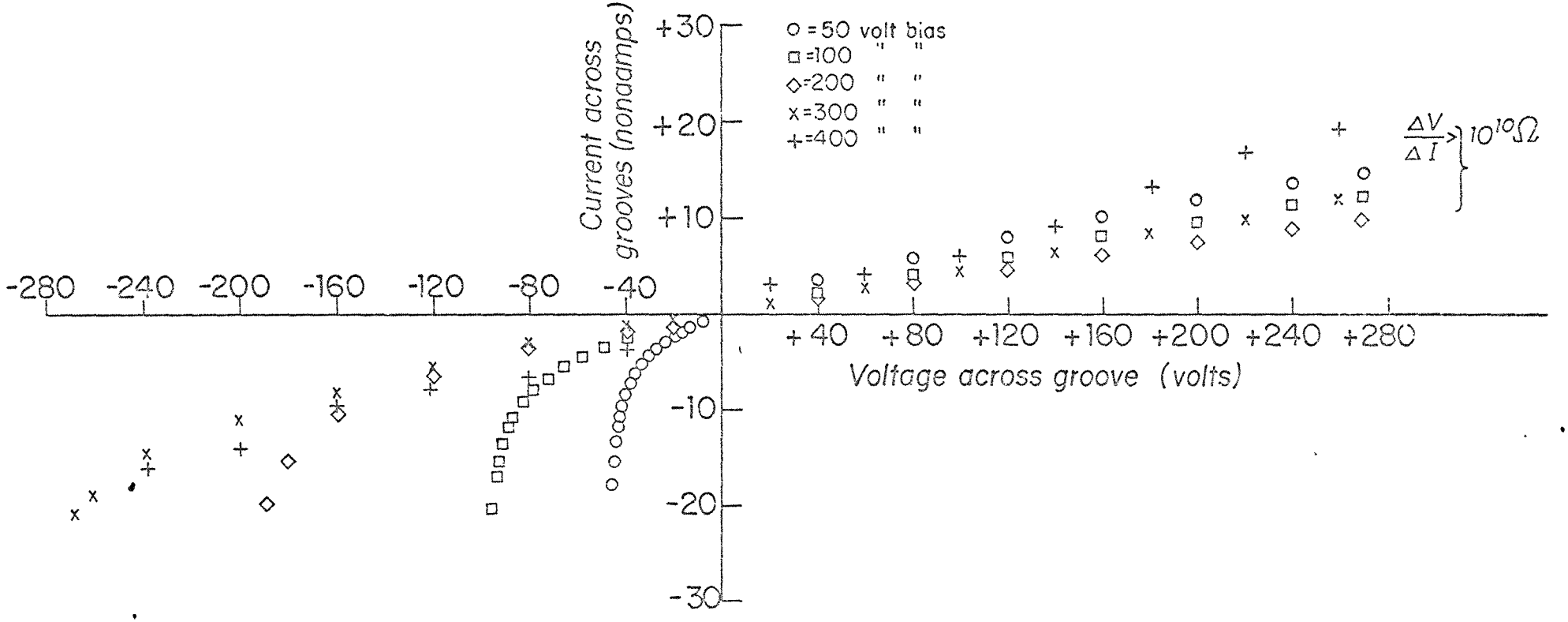

Figure XXI

MATRIX OS-2

P-SIDE GROOVE RESISTANCE AT 500 VOLTS BIAS

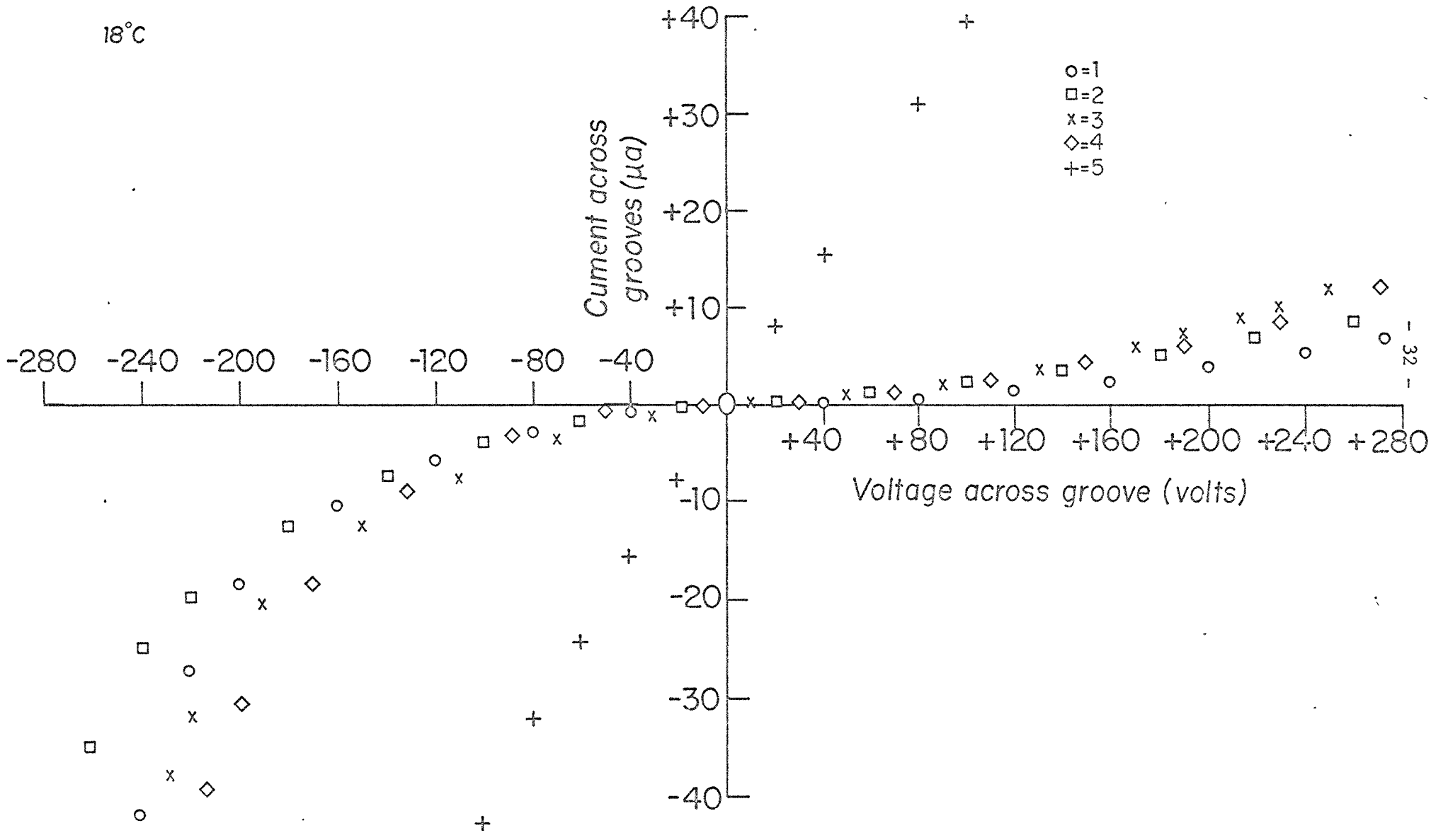

earlier application of this configuration to a smaller diode which was immediately encapsulated in polyurathane varnish following its construction. All efforts to obtain high n side groove resistance for this unit were futile. However, the p side groove resistance for this early unit can be seen in Figure XXII to be in the 10^9 ohm range 5 months after fabrication.

3. Position sensitivity of matrix to P-32 electron beam

a) Source construction

A P-32 source was used to probe the matrix surface in testing it for position sensitivity. The source schematic is given in Figure XXIII. A 1 cm long, 1 mm inside diameter, polyethylene tube was loaded with about .01 cc of a 2.5 mc/cc solution of P-32, sealed at both ends with a paraffin bead and mounted in a holder consisting of sheaths of teflon, aluminum and lead.

Particle leakage from the holder stem was negligible. The output of the source in its holder was examined with a thin window lithium drifted diode (Technical Measurements Corp.). Variation of count rate versus discriminator (integral mode) baseline setting is shown in Figure XXIV. A similar holder has recently been constructed of Mallory 1000 metal (90% tungsten, 6% nickel, 4% copper) in preparation for low energy gamma-ray measurements. A positioning carriage with two degrees of freedom has also been constructed for the source holders, allowing a source while in the test box to be positioned from the outside at a chosen point over the matrix. This can be seen in Figure XVI.

b) Results

Figure XXV presents results of initial tests of the position sensitivity of the matrix in detecting the region of incidence of the approximately 1 mm diameter beta particle beam from the collimated P-32 source described above. The collimator was placed close to the surface of the device. The n and p side strips were monitored in tandem with a charge sensitive preamplifier, amplifier, discriminator, and scaler. The six n-side strips are indicated vertically at the left side of the figure, the p side strips at the bottom. The length of the hatched bars indicates the number of counts recorded in one minute at each of the lw strips, the scale being at the top and at the right side. The source was positioned visually above the matrix n side when these particular measurements were made, hence the rough indication in the legend of source position.

In Figure XXVI, the source position has been changed and the matrix boundary is indicated. Good correlation is obtained between the known source location and that indicated by the relative number of counts at each row and column. A resolution of within (3 x 3)mm^2 is demonstrated on this basis.

4. Evaluation of matrix response to low energy gamma-rays using detector cooling

The evaluation of matrix response to low energy gamma-ray emitting isotopes (below 60 KeV) is not complete at this writing but will be completed for several units before the end of this contract year.

Figure XXII

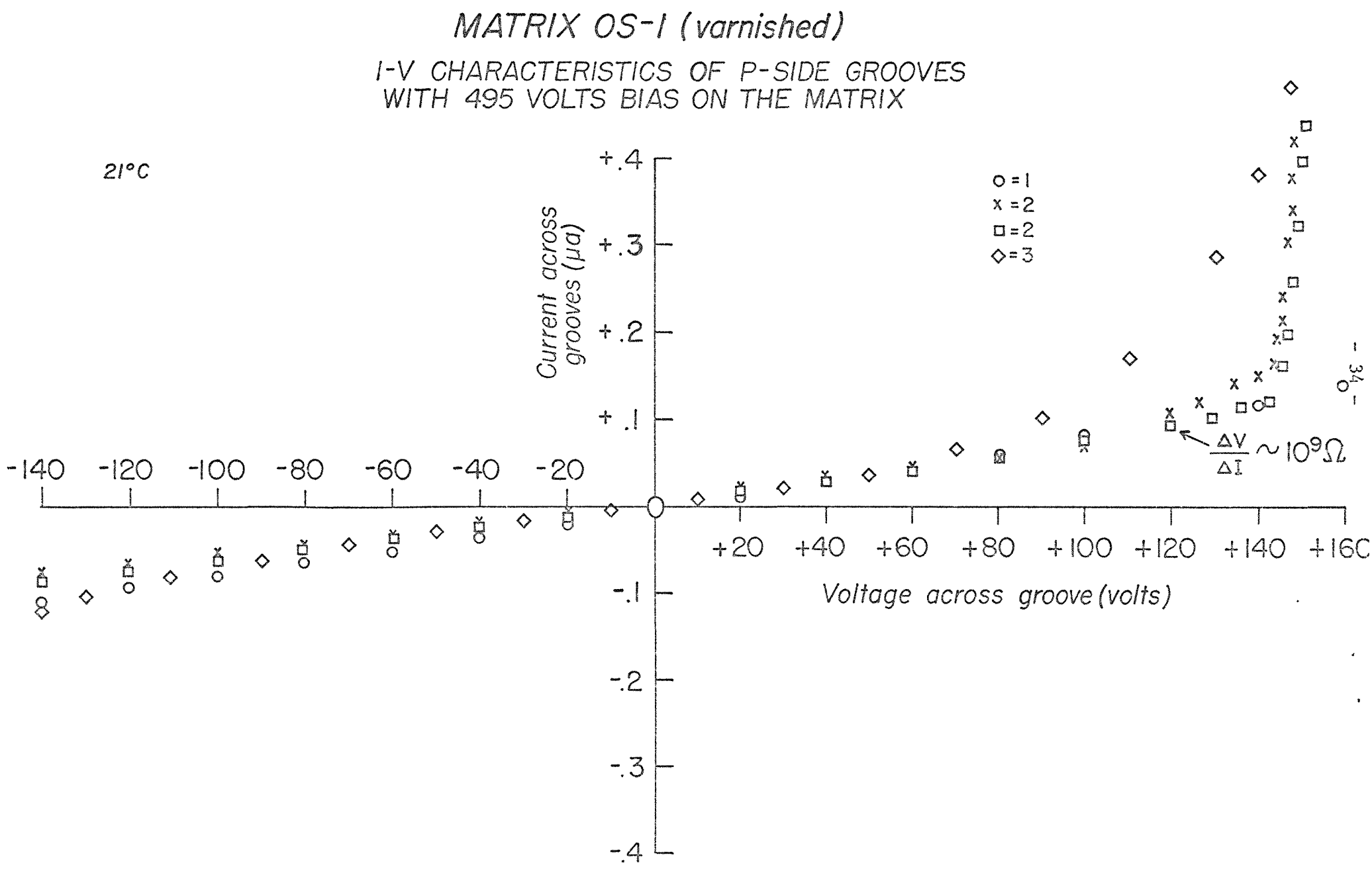
MATRIX OS-1 (varnished)
I-V CHARACTERISTICS OF P-SIDE GROOVES
WITH 495 VOLTS BIAS ON THE MATRIX
21°C
Current across grooves (μa)
+.4
+.3
+.2
+.1
-.1
-.2
-.3
-.4
-140
-120
-100
-80
-60
-40
-20
+20
+40
+60
+80
+100
+120
+140
+160
Voltage across groove (volts)
o = 1
x = 2
□ = 2
◇ = 3
ΔV/ΔI ~ 10⁹Ω
3¼

Figure XXIII

COLLIMATED P-32 BETA SOURCE HOLDER

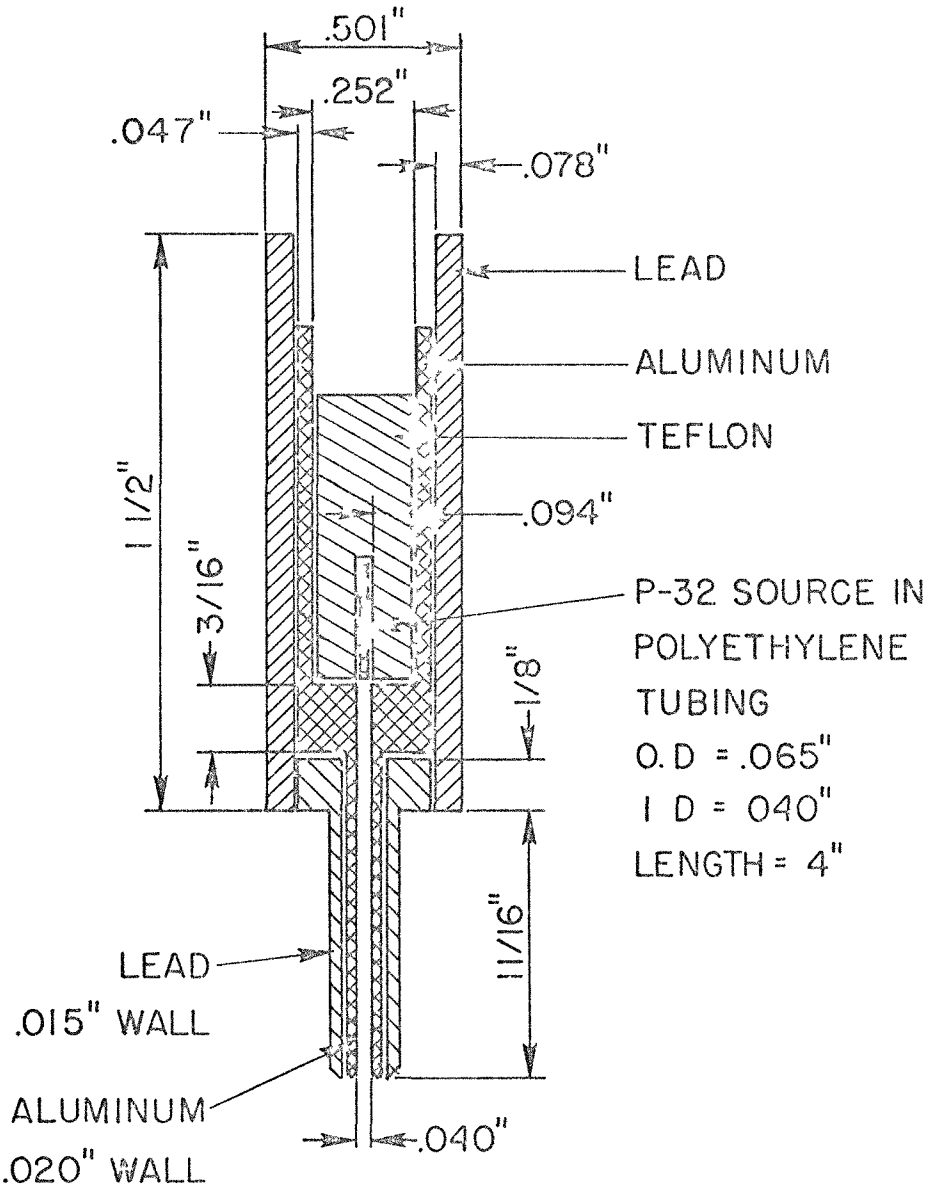

Figure XXIV

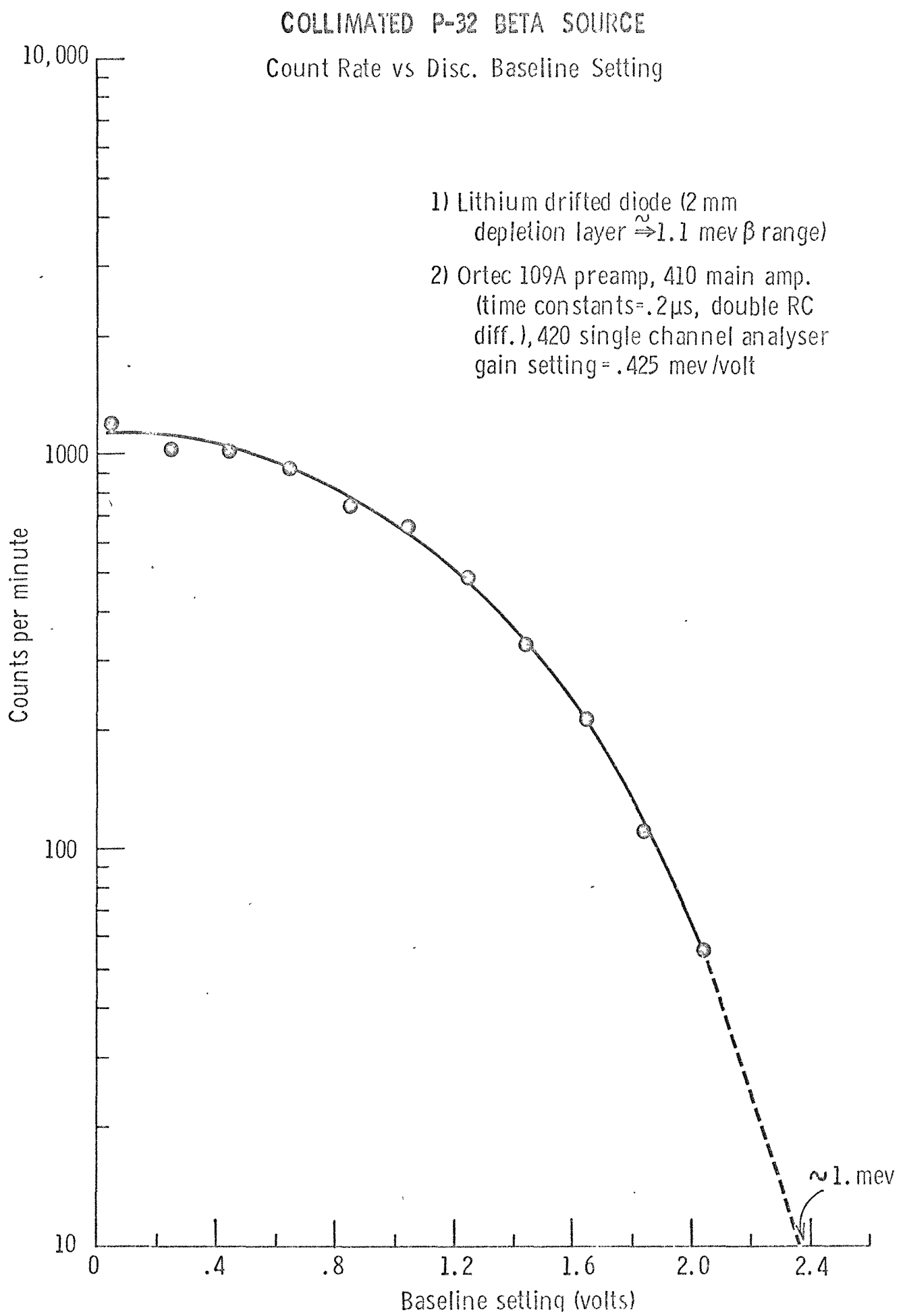
COLLIMATED P-32 BETA SOURCE
Count Rate vs Disc. Baseline Setting
1) Lithium drifted diode (2 mm depletion layer ≃ 1.1 mev β range)
2) Ortec 109A preamp, 410 main amp. (time constants = .2μs, double RC diff.), 420 single channel analyser gain setting = .425 mev/volt
10,000
1000
100
10
Counts per minute
0
.4
.8
1.2
1.6
2.0
2.4
Baseline setting (volts)
≃ 1. mev

Figure XXV

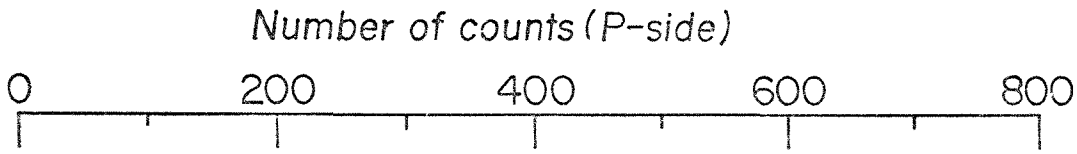

20°C

SOURCE POSITION
n-side - row # 5 (near #4)
P-side - column #4 (near # 3)
1 minute count time - 250 volts bias

	P-side count	n-side count
lower level	.68 volts	.67 volts
Δ E(window)	10 volts	10 volts

Main AMP. .2μs. double RC time constants, .2μs. integ. time constant

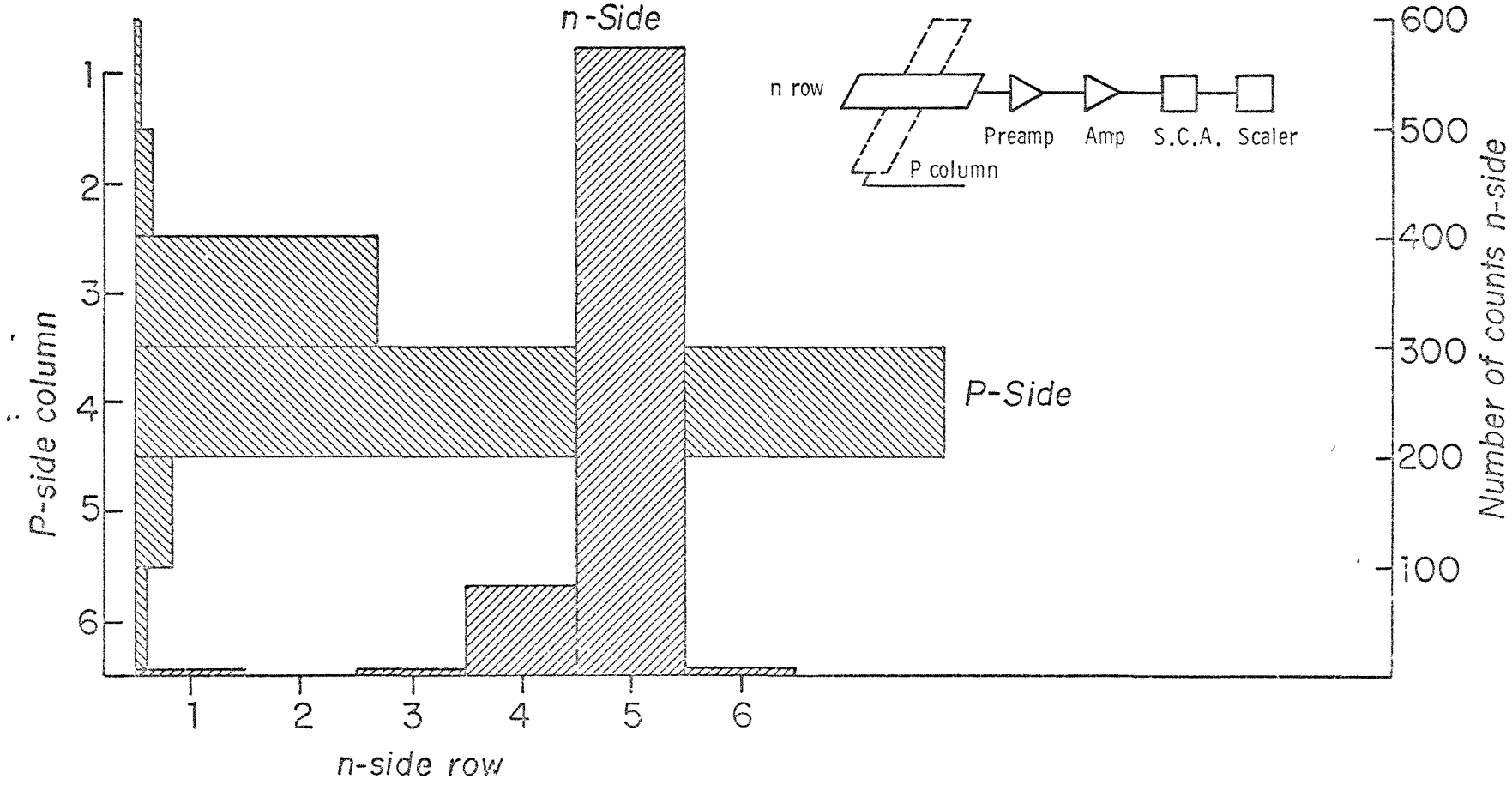

Figure XXVI

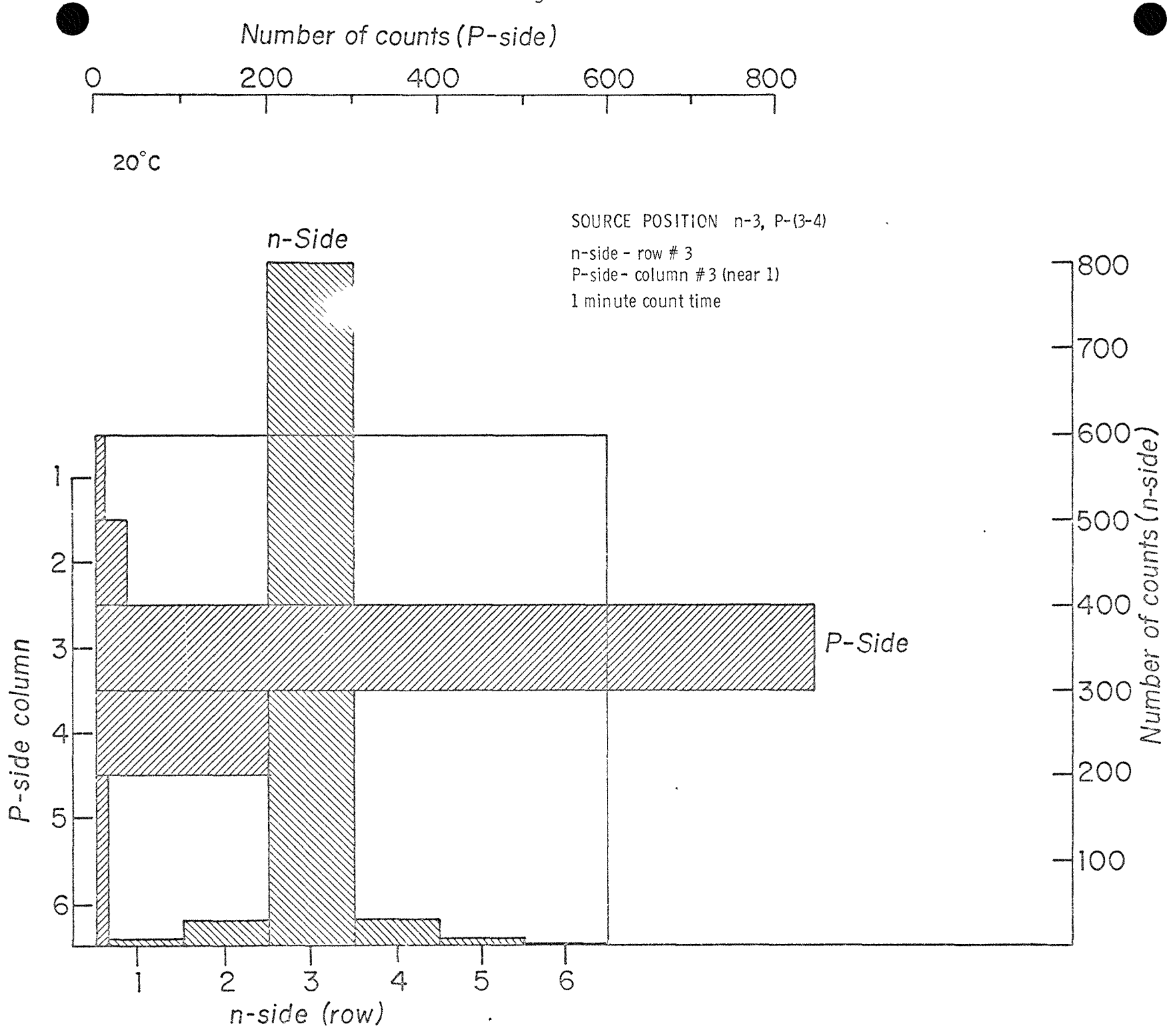
Number of counts (P-side)
0
200
400
600
800
20°C
SOURCE POSITION n-3, P-(3-4)
n-side - row # 3
P-side - column # 3 (near 1)
1 minute count time
n-Side
P-Side
P-side column
n-side (row)
Number of counts (n-side)
1
2
3
4
5
6
100
200
300
400
500
600
700
800

To be able to detect, say, I-125 gamma-rays (80% 27.4 KeV), detector cooling is required to depress noise levels (FWHM) well below signal levels. The initial set up being used for this consists of a polyurethane foam dry-ice reservoir through which is passed a number of turns of copper capillary tubing (1/8 inch O.D.) carrying the dry nitrogen which is flowed through the test box (Figure XVI) during measurements. For a gas flow rate of ∿9 c.f.h., a measured exit temperature of -88°F is obtained. At present, only an initial indication has been obtained of the effectiveness of this arrangement for cooling the matrix. This was done through measurements made when the insulation around the test box was preliminary. The parameters observed were the noise (FWHM) at the individual electrode strips along with the corresponding zero count (1 minute) integral discriminator baseline settings for the noise (i.e., the baseline setting for each electrode strip at which less than ten noise pulses are counted in one minute. The two quantities should change in roughly the same proportion if, as expected, the noise is Guassian. Such was found to be the case. With the matrix temperature reduced around 10°C below room temperature, a 40-50% improvement in both figures was obtained. This is the order of change which would have been predicted on the basis of the observed change in leakage current through the $\sim I_L^{1/2}$ dependence of the noise (18).

5. Evaluation of commercially produced instrumentation for use with matrix arrays

It was stated in a previous proposal (AEC Proposal 1966 and 1967) that a unit produced by Canberra Industries was under consideration for use with two dimensional matrix arrays. Six of these units were finally obtained after a number of modifications were completed. The unit (PAD813) incorporates an f.e.t. charge sensitive preamplifier, main amplifier, and 0 to 10 volt integral discriminator in a single width nuclear instrument module. The pulse shaping time constants in the units produced for SKI are set at 0.2 μs with double differentiation and single integration but can be changed upward to other values if required. To determine the useful limit of detector capacitance, the noise levels (FWHM) and gain versus input capacitance for the six units were measured and are shown in Figures XXVII-XXXI. For comparison, the curve measured for a standard Canberra preamplifier offered for a cost exceeding a single PAD 813 unit is also shown in Figure XXVII.

6. Effect of restorative surface treatments on matrix properties

Exposure to the room ambient eventually brought p side groove resistance down to unusuable levels (<100 KΩ). N side groove resistances, on the other hand, seemed to improve with time in room air. In an effort to recover high p side groove resistance the matrix, with electrode strips remasked, was given a number of short etches followed by deionized water rinses. The initial effect of this was to restore high p side groove resistance as intended, but with an accompanying reduction of n side resistance. Such was the case when the matrix was first fabricated until reverse bias was applied for about a day. However, this measure was unsuccessful when reapplied here as were subsequent etches followed by periods of high reverse bias in flowing nitrogen. The situation was finally corrected by extended boiling of the matrix in dionized water. The groove resistances for both n and p sides

Figure XXVII

PAD 813 UNITS

Output Noise (FWHM) vs Input Capacitance

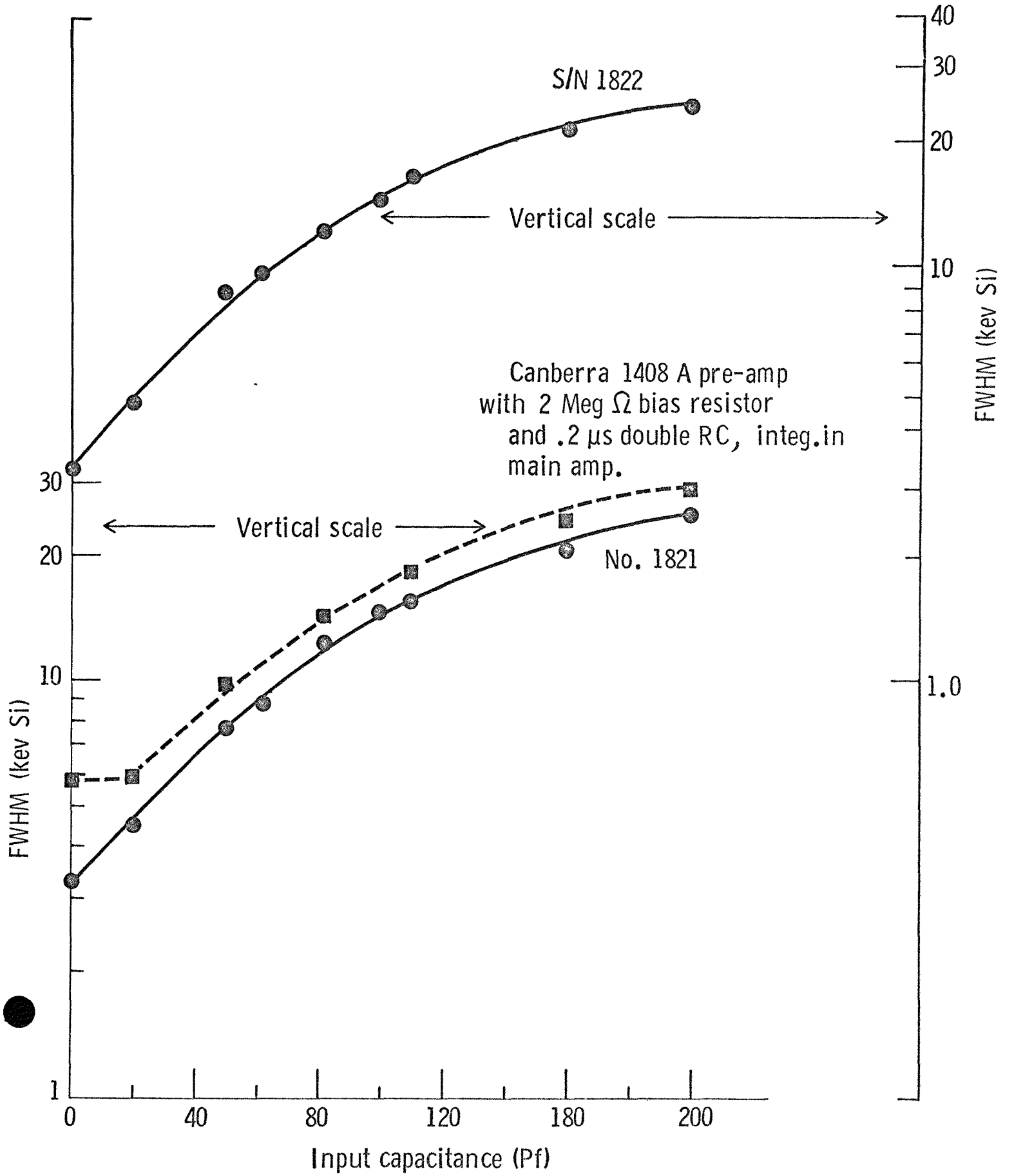

Figure XXVIII

PAD 813 UNITS

Output Noise (FWHM) vs Input Capacitance

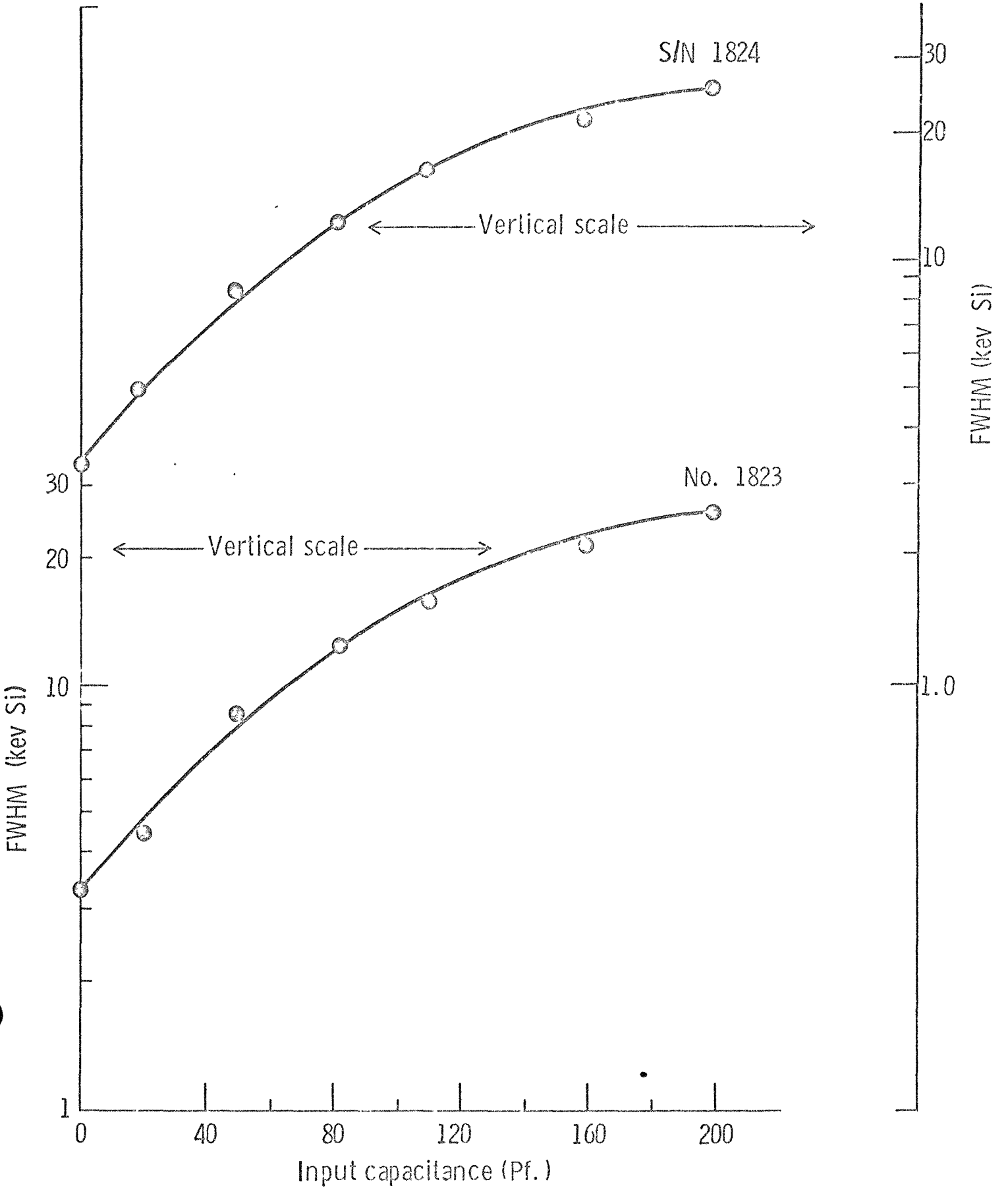

Figure XXIX

PAD 813 UNITS

Output Noise (FWHM) vs Input Capacitance

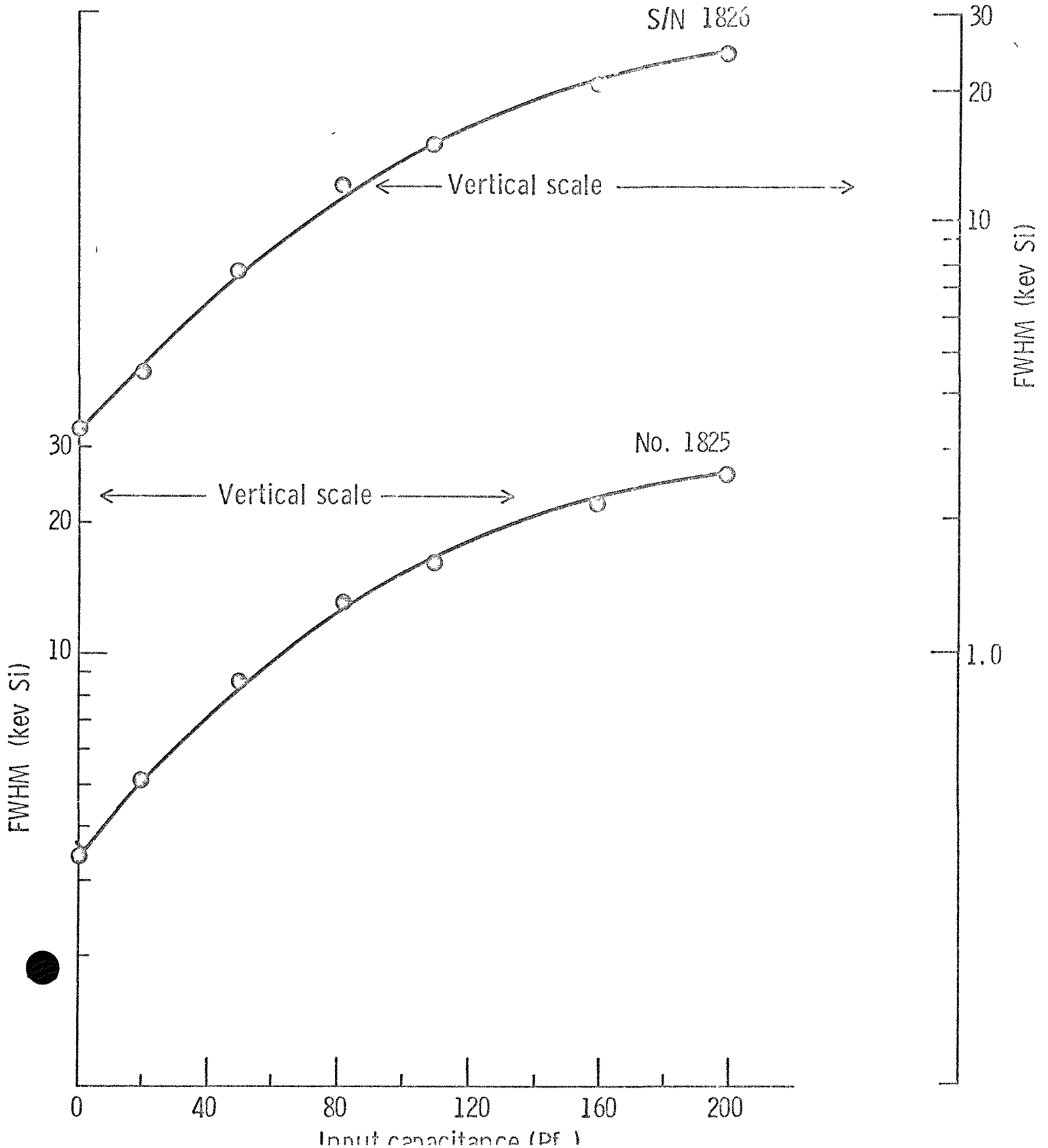

Figure XXX

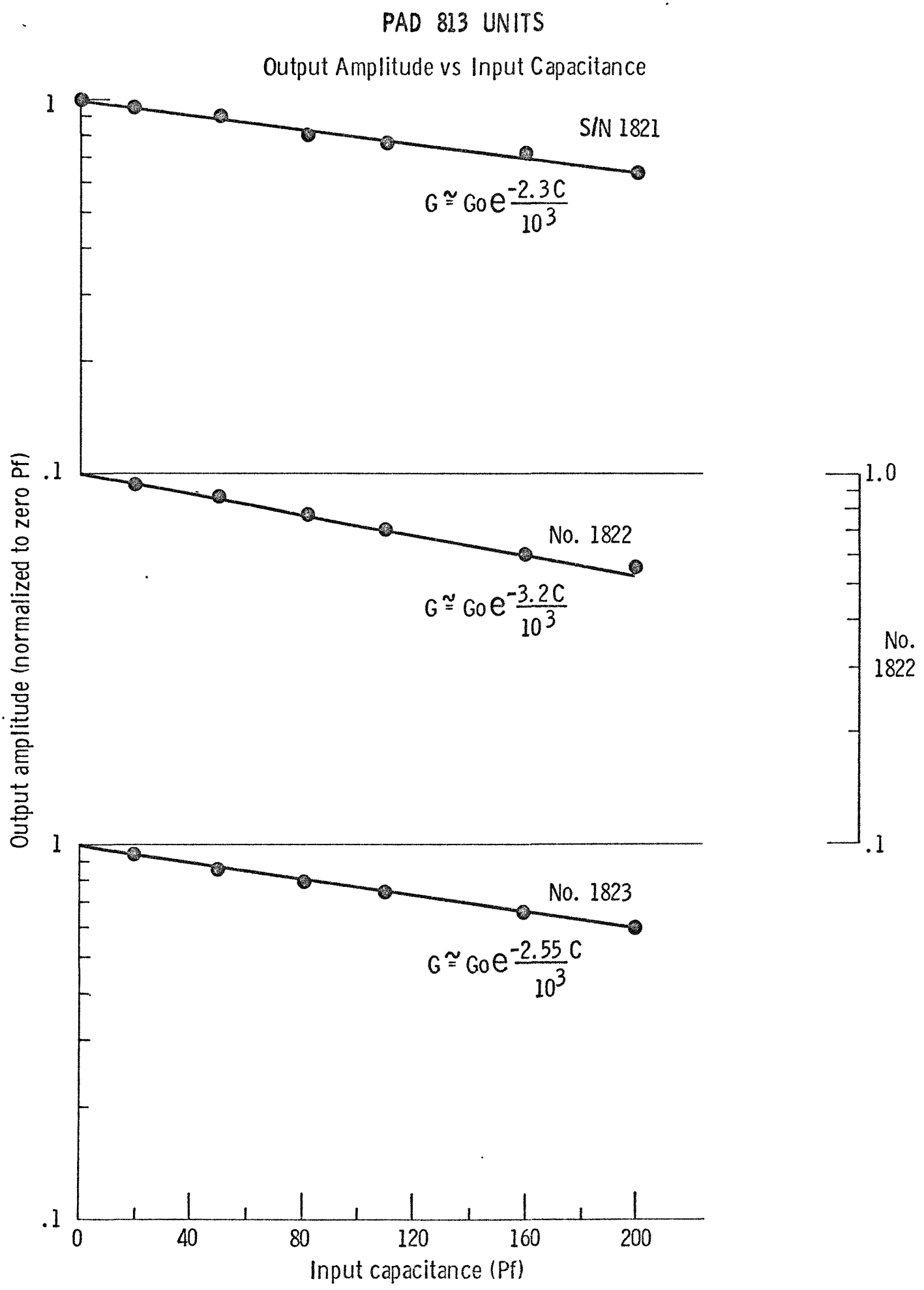
PAD 813 UNITS
Output Amplitude vs Input Capacitance
S/N 1821
$G \cong G_o e^{\frac{-2.3C}{10^3}}$
No. 1822
$G \cong G_o e^{\frac{-3.2C}{10^3}}$
No. 1823
$G \cong G_o e^{\frac{-2.55C}{10^3}}$
Output amplitude (normalized to zero Pf)
1
.1
0
40
80
120
160
200
Input capacitance (Pf)
1.0
.1
No. 1822

Figure XXXI

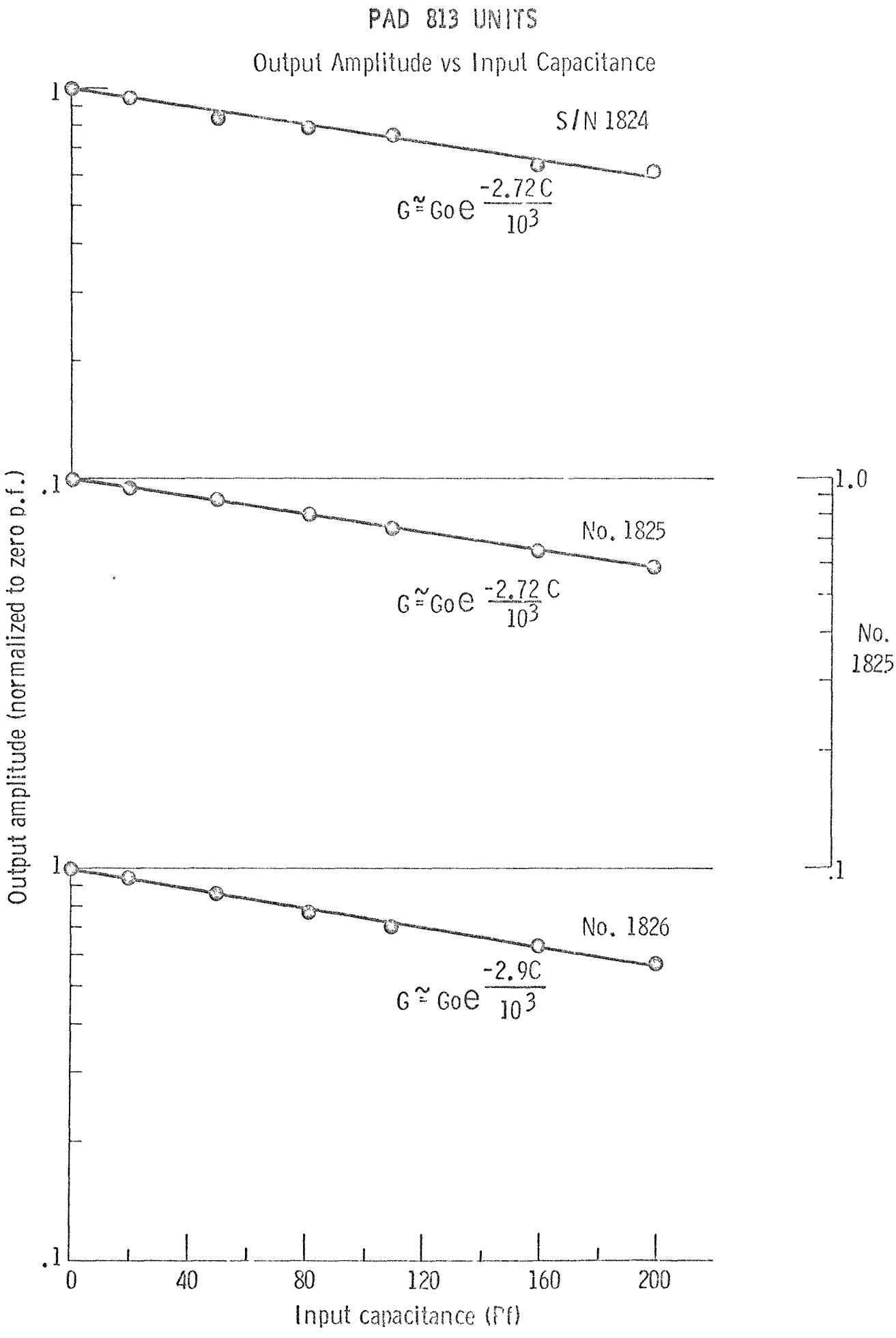
PAD 813 UNITS
Output Amplitude vs Input Capacitance
S/N 1824
$G \cong G_o e^{\frac{-2.72C}{10^3}}$
No. 1825
$G \cong G_o e^{\frac{-2.72C}{10^3}}$
No. 1826
$G \cong G_o e^{\frac{-2.9C}{10^3}}$
Output amplitude (normalized to zero p.f.)
1
.1
0
40
80
120
160
200
Input capacitance (Pf)
1.0
.1
No. 1825

along with noise levels were measured for the matrix after this treatment was completed. For up to 200 volts across the grooves, all grooves on both sides of the matrix have effective resistances in excess of 10^8 ohms at 500 volts reverse bias. All but one (n side) are over 5 x 10^8 ohms. Noise levels for the individual strips are about as low as originally measured. Representative data are shown in Figures XXXII-XXXIV.

Following the surface treatments, the position sensitivity of the matrix was remeasured, using a collimated P-32 beta source, and found to compare to the original quality for the n side while p side resolution spread to about 5 mm. Significantly, an accompanying loss in the counting sensitivity was observed. Both effects are attributed to a thickening of the n side dead layer as a result of a shift in the lithium distribution in the absence of reverse bias. This explanation is compatible with the diffusion constant of lithium in silicon at room temperature and can usually be reversed for diodes of conventional geometry upon extended application of reverse bias. However, while no concerted effort has been made to apply this remedy since other devices are in construction, there is some indication that the geometry of the device may preclude the effectiveness of the remedy, and instead require storage under reverse bias or at refrigerator temperature at the outset. (From 20°C to 0°C the diffusion constant of lithium in silicon drops by over a factor of ten (10). Future work with these devices will include attention to this area.

B. Experimental Tests of Ultrasonically Bonded Electrical Lead Wires to Diode Electrodes

1. Applications planned

The connection of permanent lead wires to diode electrodes is often preferable to the frequently used pressure type contact. Ultrasonic bonding is a widely used alternative in many cases, especially in industry. Since the procedures involved are straightforward, the particular advantages of this technique were sought for applications at SKI. These pertain to the fabrication of miniature diodes which is discussed below, and to the connection of electrical lead wires between a diode matrix and its preamplifiers and between other matrix units in an array.

In the case of miniature diodes, the aim was to provide electrical contacts while obtaining a reduction in the mass of nearby electrical lead wires whose scattering contribution in an irradiated medium can significantly perturb the response of a small diode (15). A 1040 TSL ultrasonic bonder produced by Sonobond Corp. was obtained for this work.

Since aluminum wire was considered most useful for the intended applications, bonding only with it was investigated and then only for the substrates to be used.

2. Results

Strong, reproducible bonds were obtained between .010" aluminum wire and electroless nickel electrodes of 10 and 20 micron thickness on silicon and between .005" and .010" aluminum wire and bare, etched silicon.

Figure XXXII

MATRIX OS-2

GROOVE RESISTANCE OF SINGLE n SIDE GROOVE vs REVERSE BIAS
AFTER SURFACE TREATMENT

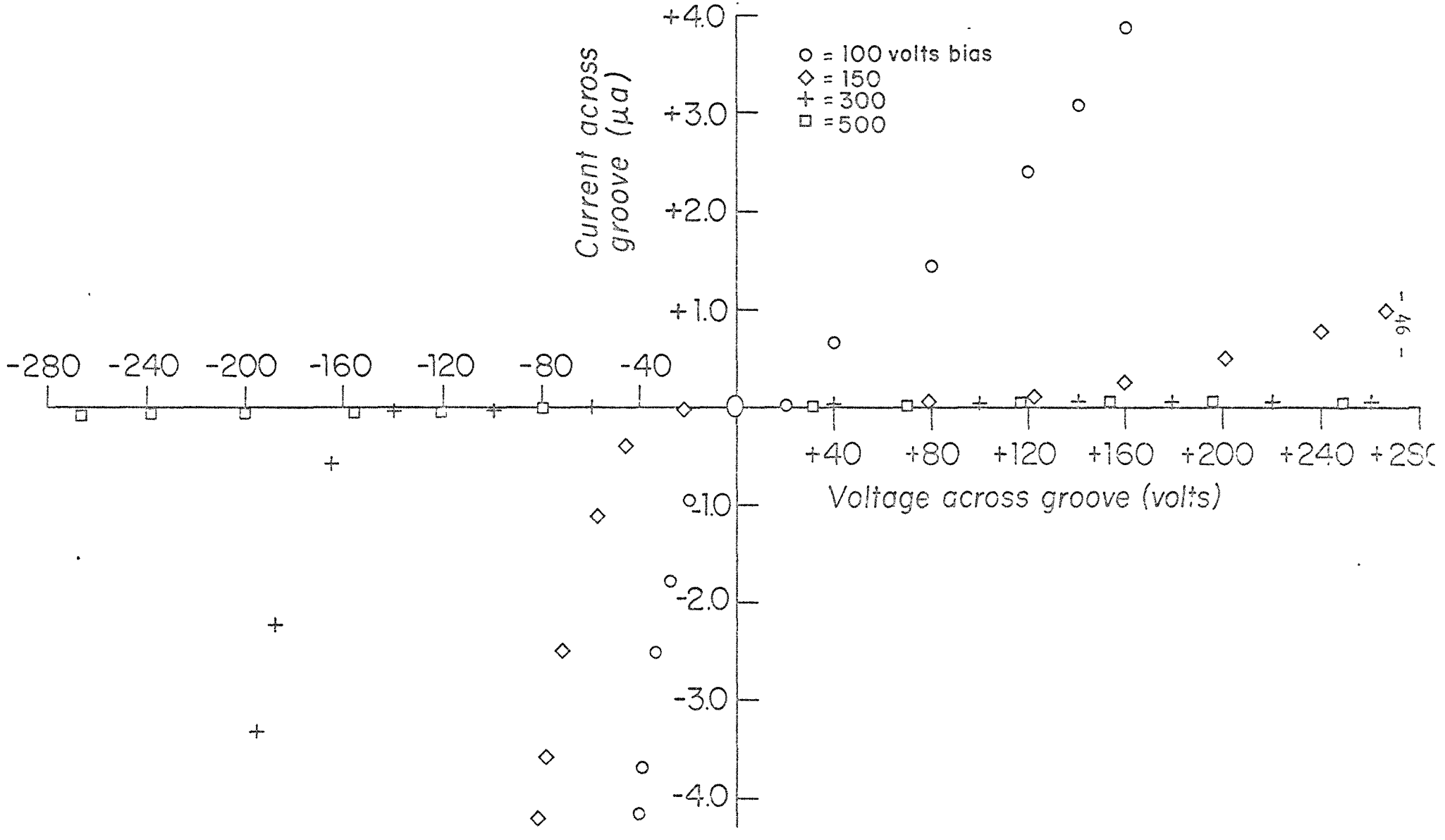

Figure XXXIII

MATRIX OS-2

GROOVE RESISTANCE OF SINGLE P SIDE GROOVE vs REVERSE BIAS
AFTER SURFACE TREATMENT

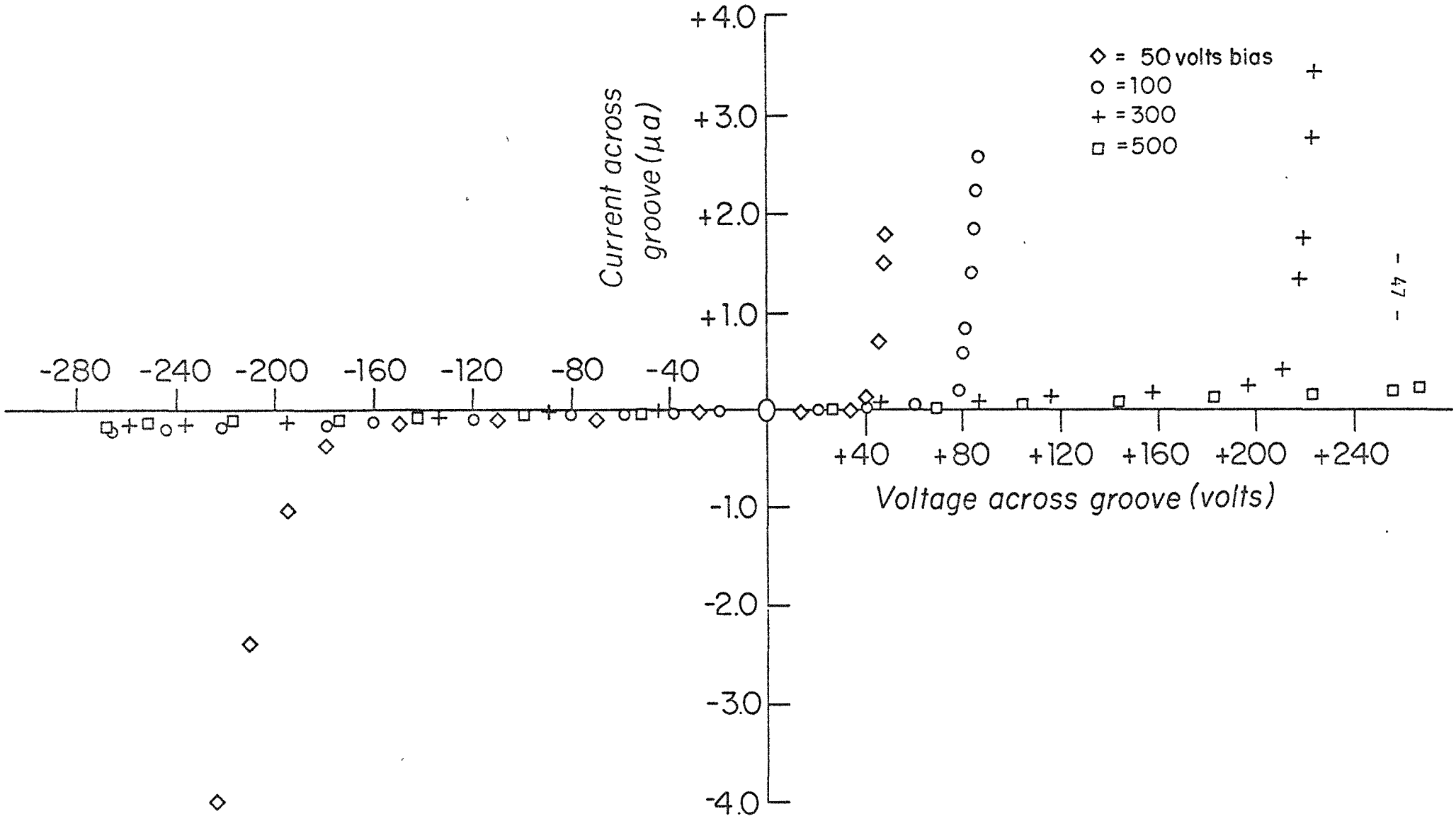

Figure XXXIV

MATRIX OS-2

NOISE MEASUREMENTS OF INDIVIDUAL n SIDE ELECTRODE STRIPS vs REVERSE BIAS AFTER SURFACE TREATMENT

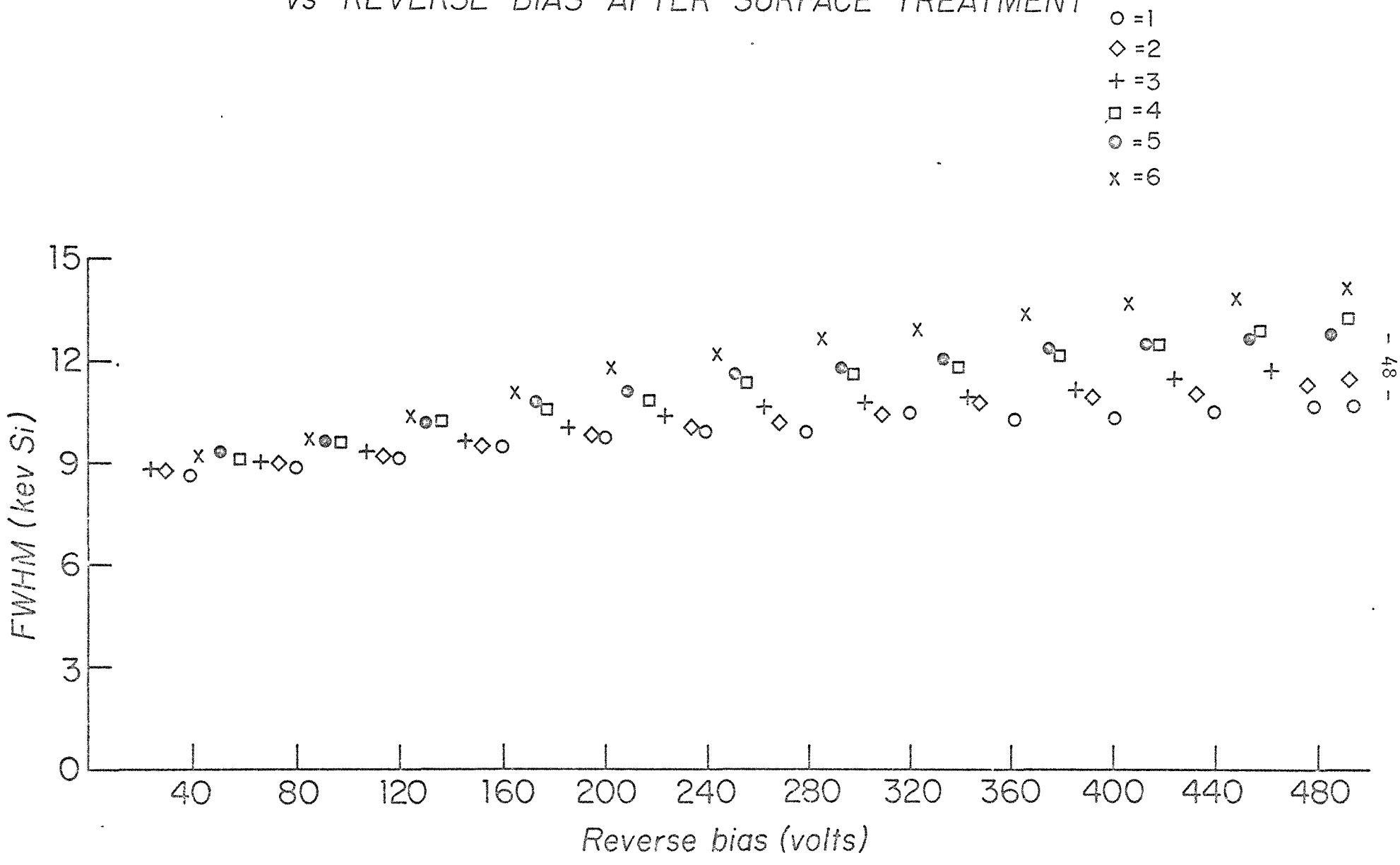

(Nickel electrodes are most convenient for use as matrix electrodes due to their good adhesiveness and low chemical reactivity-features which enter into the chemical surface treatment of a diode.) The aluminum wire used was annealed, 99.999% pure. Conventionally, "peel" and "pull" strength are used in characterizing bond quality, but it is sufficient here to note that when the variables were properly set, bond strengths usually matched wire strength or film adhesive strength pulling in directions nearly perpendicular to the surface. Attempts to bond to 1 micron thick nickel on silicon were unsuccessful both at SKI and Sonobond Corp. to which specimens were sent for trial.

C. Construction of Miniature Diodes with Ultrasonically Bonded Leads

In a previous proposal (AEC Proposal 1966-1967), miniature pn junction silicon diodes were discussed with reference to possible use in absorbed dose measurements with Co-60 gamma-rays as well as with high energy electrons. Commercially available units which have been tried have not proved suitable (15). The fabrication of two promising types of miniature diodes at SKI was made practical through the use of ultrasonic bonding of lead wires. The first is of the "wrap around junction" type [whose construction is discussed in a previous report (15)], having junctions on fire faces of an approximately two mm cube. .010" aluminum lead wires were bonded directly to the silicon without an intervening plated electrode. The low resistivity of the outer n type faces and small dimensions make this feasible for both side of the junction. The other type consists of a (1 x 1 x .25 mm) rectangular pn silicon diode with .005" aluminum leads also bonded directly to unplated p and n sides. Both devices are shown in Figure XXXV next to a match head. A half dozen of these were made initially for evaluation. The construction of the smaller device is especially simple, well over a hundred being obtainable from a single wafer. Due to handling problems, it is not expected that dimensions less than (.5 x .5 x .25) mm can be obtained without making their fabrication impractical. These devices will be suitable as in vivo probes after phantom evaluation under Co-60, high energy electrons and x-ray machines. These measurements will be complete by the end of this contract year. A point check made at 150 KVCP (HVL . 66 Cu) to determine output level indicates a sensitivity of about 2 nanoamps/r/min. for the wrap-around geometry in short circuit (zero bias) mode and about 60 picoamps/r/min. for the smaller type. For comparison, the response of an air ionization chamber with a one cubic centimeter collecting volume is about 6 picoamps/r/min. at the same energy.

Figure XXXV

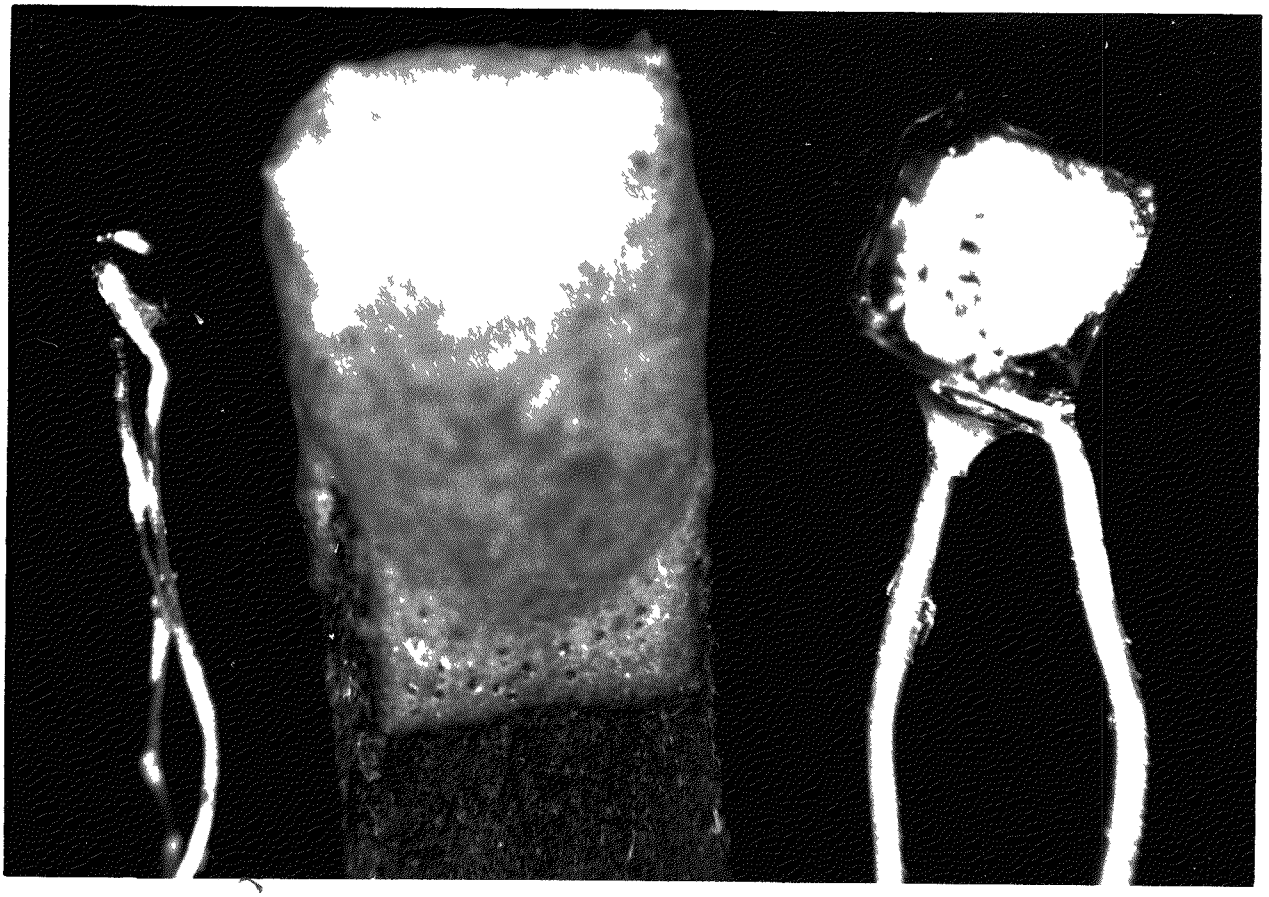

Miniature Diode

1. Dyke, W. P., Advances in Field Emission, Sci. Am. 210:No. 1, 108, 1964.

2. Goldstein, N., Tochlin, E., and Miller, W. G., Millrad and Megarad Dosimetry with LiF, Health Physics, 14:159, 1968.

3.* Pinkerton, A., Alsop, B., Weiss, H. and Epp, E. R., Dosimetry Studies with High Intensity Field Emission Electron Source, Presented AAPM Meeting, December, 1967 (abstract).

4.* Pinkerton, A., Alsop, B., Weiss, H., and Epp, E. R., Dosimetry of a High Intensity Field Emission Electron Source, Presented Radiation Research Society Meeting, April, 1968 (abstract).

5. Bess, L., Ovadia, J. and Valassis, J., External Beam Current Monitor, Rev. Sci. Instr. 30:989, 1959.

6. Hayne, J. F., Jennings, R. E. and Rand, R. E., A Null Method for Calibrating Faraday Cups, Nuclear Instr. and Methods, 24:456, 1963.

7. Ebert, P. J. and Lasher, D. R., Fast Sensitive Noninterrupting Monitor for Nanosecond Pulsed Beams, Rev. Sci. Instr., 32:1347, 1961.

8. Sub-Committee on Radiation Dosimetry, AAPM-Protocol for the Dosimetry of High Energy Electrons, Phys. Med. & Biol., 11:505, 1966.

9. Pinkerton, A., Holt, J. G., Laughlin, J. S. and Almond, P. R., The Direct Intercomparison of Absorbed Dose by Thermoluminescent Dosimetry, Proc. of International Conference on Luminescence Dosimetry, Stanford, June, 1965.

10. Fowler, J. F., Neutrons in Radiotherapy: Slow Neutrons, Fast Neutrons, and Other Heavy Particles, Proc. IAEA Symp. on Biological Effects of Neutron and Proton Irradiations, Vol. II, 185, Pub. IAEA, Vienna, 1964.

11. Andrews, J. R., and Hollister, H., Fast Neutron Beam Radiotherapy: Status and Prospects, Radiology, 99:954, 1967.

12. Moroson, R. L., Clinical Experience of 6 MeV Fast Neutrons in Radiotherapy, Presented Radiation Research Society Meeting, April, 1968.

13. Bewley, D. K., A Comparison of the Response of Mammalian Cells to Fast Neutrons and Charged Particle Beams, Rad. Res., 34:446, 1968.

14. Caley, R., and Dahler, A., An Automatic Depth Dose Plotter, Presented at the Radiological Society of North America Meeting, Chicago, 1966.

15. Annual Progress Report, Biological and Clinical Dosimetry, AEC Contract AT(30-1)3510, 1966-67.

16. Miller, G. L., Pate, B. D., and Wagner, S., Production of Thick Semiconductor Radiation Detectors by Lithium Drifting, IEEE Trans., vol. NS-10, 220, 1963.

*reprints accompany this report

17. Hayashi, I., Kern, H., et al., A Vacuum Encapsulated Lithium Drift Detector Telescope, IEEE Trans. Vol. ND-13, 214-220, June, 1966.

18. Goulding, F. S., and Hansen, W. L., Leakage Current in Semiconductor Radiation Detectors and its Influence on Energy Resolution Characteristics, Nuc. Instr. Meth., 12:249-262, 1961.

19. Pell, E. M., Diffusion of Li in Si at High T and the Isotope Effect, Phys. Rev., 119:3, 1960.